TWINS IN BARIUM TITANATE†

Aleksander Rečnik
Jožef Stefan Institute, Jamova 39, 1000 Ljubljana, Slovenia

† This paper is dedicated to the late Professor Dr. Drago Kolar

Received 10–01–2001

Abstract

On the example of (111) twins in cubic $BaTiO_3$ it has been shown that reducing sintering conditions influence the propensity of the grains to twin, i.e. the formation of a hexagonal stacking sequence in a form of Ti_2O_9 coordination groups. Furthermore, Ti_2O_9 groups are a common for both (111) cubic twins and the hexagonal polymorph itself. In the literature, there is no experimental evidence that would explain the nature of cubic–hexagonal phase transformation mechanism. This phase transformation may be shifted far below the normal transition temperature when processing under reducing conditions. While Ti^{3+} ions stabilise the hexagonal stacking (either in twins or the hexagonal phase) at lower temperatures, they are no longer necessary close to a normal transition temperature. This observation suggests that (111) twins in $BaTiO_3$ are preparatory stage of cubic–hexagonal phase transformation, where the phase transformation can be controlled by a suitable chemical environment that stimulates or prevents the formation of hexagonal stacking.

Introduction

Barium titanate based ceramics are important in the production of many electronic components, such as capacitors and positive temperature–coefficient thermistors. The nature of these materials depends on chemical and microstructural heterogeneities. The grain size distribution in $BaTiO_3$ ceramic materials is to a great extent determined by the occurrence of an anomalous grain growth. Such a controlled exaggerated grain growth may be desirable in the production of barrier–layer capacitors, but intentionally avoided in the production of multilayer capacitors and conventional $BaTiO_3$ dielectrics, which require a fine–grained texture.

Exaggerated grain growth in $BaTiO_3$ ceramics is believed to be triggered via the formation of (111) twins. However, the complete understanding of an anomalous grain growth in $BaTiO_3$ ceramics remains elusive. The (111) twins in the starting $BaTiO_3$ have

been considered by Eibl et al.[1] as one of the possible reasons for such growth anomalies and it has been reported by Oppolzer and Schmelz[2] that nearly all anomalously grown grains, grown below the eutectic temperature, contained parallel (111) twins boundaries extending throughout the grains. Growth mechanisms for *lamella–like* twinned grains have been studied extensively by many authors: Schmelz and Thomann,[3] Kästner et al.[4] although the formation mechanism of these planar faults (twins) is not understood.

To study the nucleation mechanism of (111) twins one must commence not only with a detailed information about the preparation conditions under which they form, but also a deep understanding of about their structural and compositional properties. In the last three decades several structural models for the coherent (111) twin boundary have been proposed, while the experimental data capable of verifying any of these models was lacking, leaving their real structure and nucleation mechanism ambiguous.

In this review nucleation mechanism for (111) twins will be presented in terms of their atomic structure and composition. Individual sections of this paper are upgrading the understanding of the crystal structure, twinning and the formation of some structural peculiarities in $BaTiO_3$. Firstly, we will focus on three most important polymorphs of $BaTiO_3$ (tetragonal, cubic and hexagonal) and their twins. A short literature review is a compilation of studies mainly related to (111) twins in the cubic and hexagonal phases, which were processed far below the cubic–hexagonal transition temperature in reducing sintering conditions. The materials for this study were prepared by a conventional mixed oxide powder technique under different sintering conditions.

The local structure of the (111) twin boundary was studied using most advanced electron microscopy techniques. The results of quantitative high–resolution transmission electron microscopy (HRTEM) and electron–energy–loss spectroscopy (EELS) methods were employed to propose a new structural model for the coherent (111) twin boundary in $BaTiO_3$. Based on these results and preparation conditions under which these defects formed a possible formation mechanism for the (111) twins in $BaTiO_3$ is suggested. The very close resemblance between the hexagonal $BaTiO_3$ phase and the (111) twins in the cubic phase, and the propensity of a hexagonal stacking to form under reducing sintering conditions, bids an explanation for the cubic–hexagonal transition mechanism.

Crystallography

Barium titanate is an oxide with an equimolar ratio of BaO and TiO_2. $BaTiO_3$ is one of a few materials exhibiting ferroelectric behaviour, and as such, it is widely used in the electronics industry. The crystal structure of ferroelectric materials must lack a centre of symmetry. Out of the 32 point groups 21 are non–centrosymmetric and 20 of these are piezoelectric, which means they can be polarised under mechanical stress. Ten groups exhibit pyroelectric behaviour, meaning they develop an electric dipole when an unstressed crystal is uniformly heated or cooled, and only few materials from this group exhibit ferroelectric behaviour. In $BaTiO_3$ both polymorphs, cubic and hexagonal, show a ferroelectric behaviour, which facilitates their applicability.

Polymorphism in $BaTiO_3$

Between the cubic and the hexagonal polymorph of $BaTiO_3$ a reversible phase transformation exists in the temperature range between 1430 and 1460°C. At lower temperatures the polymorphs undergo several successive phase transitions. The most important are transitions from dielectric to ferroelectric phases that occur at about 120°C for cubic, and at −199°C for hexagonal phase. This temperature, referred to as the Curie temperature, is the delimiting temperature between dielectric and ferroelectric phases of the same compound. The most important transition from the electronic point of view is cubic–tetragonal, whereas in terms of structure this is cubic–hexagonal phase transition.

Cubic and tetragonal $BaTiO_3$

The cubic form of $BaTiO_3$ is stable between 120 and 1430°C. The cubic unit cell with dimension a = 0.4001 nm, measured at low temperatures (Megaw 1947),[5] contains one formula unit of $BaTiO_3$ with atoms in the locations as shown in Table I. $BaTiO_3$ has a primitive unit cell (space group Pm3m) with the atoms located at perovskite positions. The unit–cell dimensions are temperature dependent, so that the parameter a increases proportionally with temperature to about 0.407 nm at 1370°C (Edwards et al. 1951).[6]

The crystal structure of cubic $BaTiO_3$ in two orientations is illustrated in Figure 1. In this structure Ba atoms are coordinated with twelve O atoms, while the Ti atoms are octahedrally coordinated with six O atoms. A network of corner–sharing TiO_6 octahedra

of the perovskite structure is of the ReO_3 structural type where eight corner–sharing octahedrons with the centres placed at the corners of a cube enclose dodecahedral holes which are occupied by Ba atoms in $BaTiO_3$ structure.

TABLE I

atom	Wy	x	y	z
Ba	a	1/2	1/2	1/2
Ti	b	0	0	0
O_I	c	0	0	1/2
O_I	c	0	1/2	0
O_I	c	1/2	0	0

Atomic positions in cubic $BaTiO_3$ (Megaw 1947) [5]

This way close–packed layers of Ba and O atoms along {111} perovskite planes are formed. In such a layer every Ba atom is surrounded with six O atoms (in Figure 2). Close–packed {111} Ba–O_3 layers follow a cubic repeat sequence and are interchanged with pure Ti layers that have only a quarter of the density of the close–packed layers.

TABLE II

atom	Wy	x	y	z	D–W
Ba	a	1/2	1/2	1/2	0.0051
Ti	b	0	0	0.0135	0.0030
O_I	b	0	0	0.4760	0.0057
O_{II}	c	0	1/2	0.9850	0.0067
O_{II}	c	1/2	0	0.9850	0.0067

Atomic positions and equivalent isotropic displacements [nm^2] in tetragonal $BaTiO_3$ [7]

At room temperature $BaTiO_3$ is tetragonal with a distorted perovskite structure (space group P4mm). In this ferroelectric phase the atoms are shifted from the symmetry positions of the cubic perovskite structure along the c axis by a relatively small amount. The amounts of tetragonal shifts differ in the literature mostly due to a large interference

between the position and temperature parameters along the tetragonal c axis (Harada et al. 1970).[7] The primitive unit cell with dimensions a = 0.39945 nm and b = 0.40335 nm contains one formula unit of $BaTiO_3$ with the atoms in the locations shown in Table II.

FIGURE 1

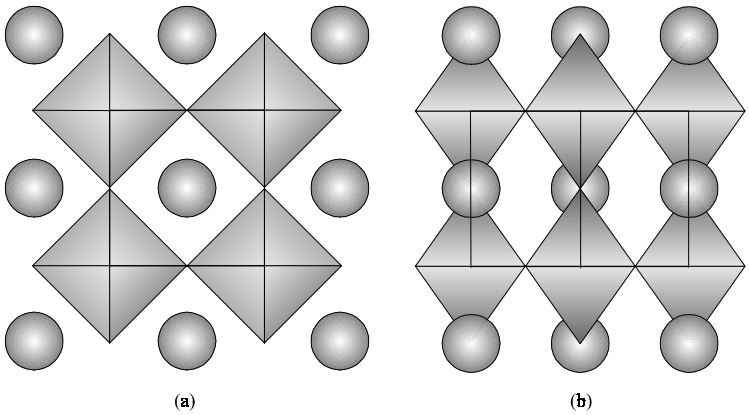

Unit cell of cubic $BaTiO_3$ viewed in (**a**) [100] and (**b**) [110] projection.

FIGURE 2

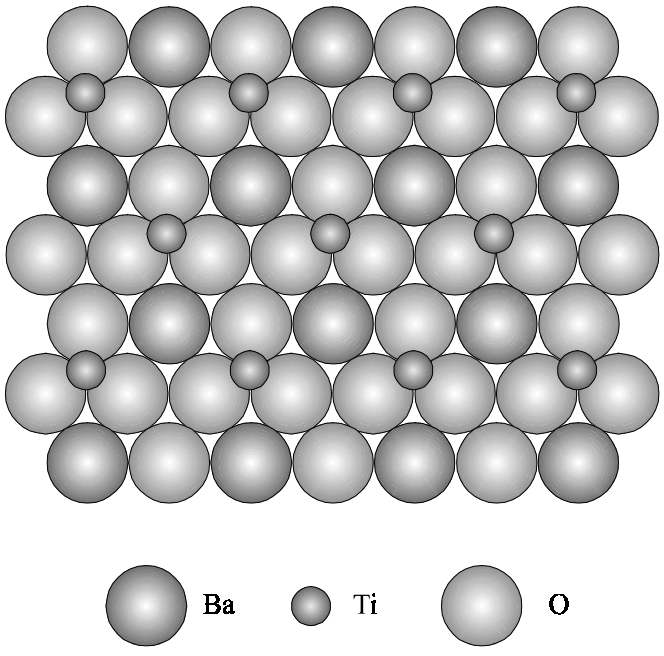

Close–packed Ba–O_3 layer with Ti sites in {111} planes of cubic $BaTiO_3$.

The elongation of the TiO_6 octahedra along the four–fold axis of the perovskite is a structural compensation for the change of ionic diameters at lower temperatures.

Growth and deformation twins

Two different types of twinning are known for barium titanate. In the tetragonal modification both growth and deformation twins are observed, while in the cubic phase only growth twins are observed. Growth twins with {111} twinning planes are formed during the grain growth at high temperatures in the cubic phase and are preserved in the tetragonal $BaTiO_3$ modification. The angle between the *c*–axes in adjacent crystals of the (111) twin is 70.53° at room temperature. First review of growth twins in $BaTiO_3$ was given by White (1955),[8] who observed *acute*– and *obtuse*–angled twins in material processed by the *Remeika* technique (Remika 1954).[9]

Deformation twins occur in polycrystalline $BaTiO_3$ below the Curie temperature as a result of cubic–tetragonal phase transition. The change in lattice parameters causes a considerable strain within the grains that results in the formation of polysynthetic twins, known as ferroelectric domains. This twinning takes place on the {101} or {100} planes. Twinning on the {101} planes produces *90° domains* (DeVries and Burke),[10] where the *c*–axes on either side of the twin boundary coincide, due to the tetragonality, at an angle 89.42° at room temperature. The unit–cell dipoles can conform to another configuration along the {100} planes, where two side–by–side *c*–axes are misaligned by 180°, known as *180° domains* or *antistructure boundaries* (Blank and Amelinckx).[11]

$BaTiO_3$ single crystals, however, do not show any deformation twinning unlike the grains of a polycrystalline material. Although the mechanical deformation is mainly equalized by the formation of ferroelectric domains, some residual stress remains in the crystals. Upon the reduction of the average grain size the number of twins per grain is reduced and the residual stress within the grains increases proportionally (Hennings 1987).[12] Thus, at grain sizes below 0.5 μm, less and less of the grains show ferroelectric domains, although the $BaTiO_3$ preserves a tetragonal symmetry.

Hexagonal $BaTiO_3$

The hexagonal form of $BaTiO_3$ is stable above 1430°C up to its melting point at 1623°C. The hexagonal unit cell with dimensions a = 0.5724 nm and c = 1.3965 nm, measured at room temperature (Akimoto et al.),[13] contains six formula units of $BaTiO_3$ with atoms in the locations shown in Table III.

TABLE III

atom	Wy	x	y	z	D–W
Ba_I	2b	0	0	1/4	0.0043
Ba_{II}	4f	1/3	2/3	0.0967	0.0052
Ti_I	2a	0	0	0	0.0067
Ti_{II}	4f	1/3	2/3	0.8463	0.0062
O_I	6h	0.5185	0.0370	1/4	0.0065
O_{II}	12k	0.8349	0.6698	0.0802	0.0066

Fractional atomic coordinates and equivalent isotropic displacements [nm^2] for hexagonal $BaTiO_3$ (Akimoto et al. 1994).[13]

FIGURE 3

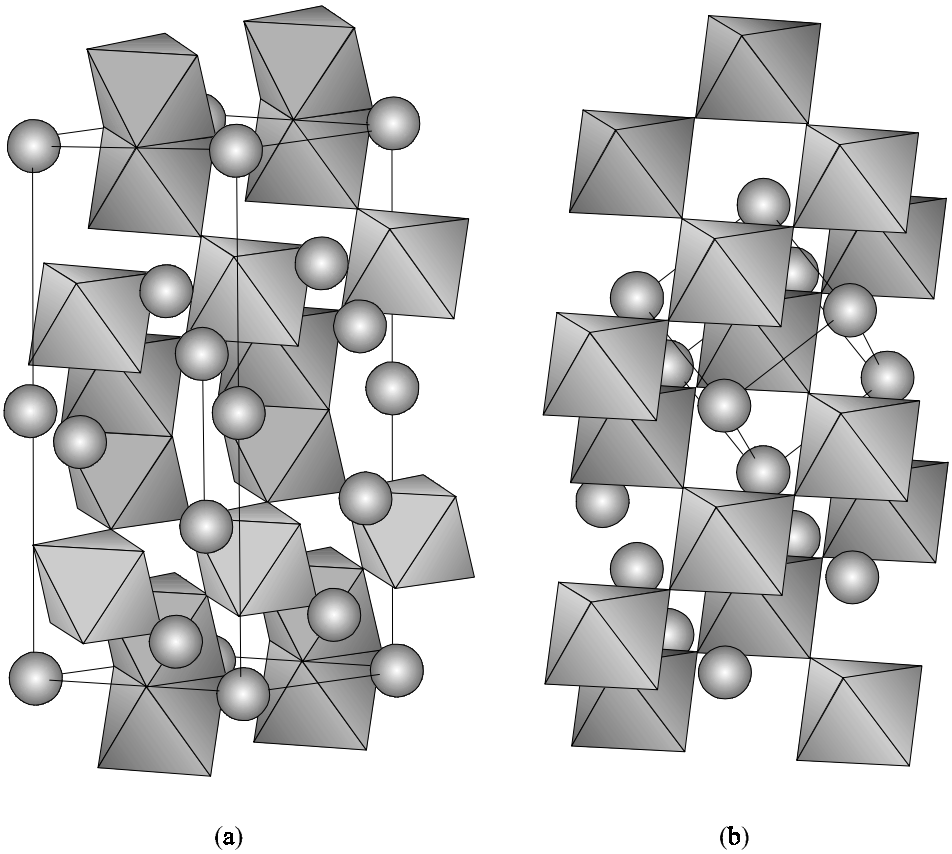

Comparison between (**a**) hexagonal and (**b**) cubic $BaTiO_3$ structures. In both unit cells Ba is placed at the origin. The stacking in hexagonal structure follows ABCACB close–packed sequence, whereas is that in cubic structure ABC (Burbank and Evans).[14]

Hexagonal $BaTiO_3$ has a primitive unit–cell (space group $P6_3/mmc$) that is in close crystallographic relationship with the polymorphic cubic form having a perovskite structure. 2/3 of the TiO_6 octahedra in the hexagonal structure occur in pairs which share faces to form Ti_2O_9 coordination groups whilst the remaining 1/3 of the TiO_6 octahedra do not share faces. The Ti_2O_9 groups are linked to TiO_6 groups by corners throughout the structure (Burbank and Evans).[14] In this structure the perovskite {111} close–packed Ba–O_3 layers are identical to the {0001} planes of the hexagonal phase.

FIGURE 4

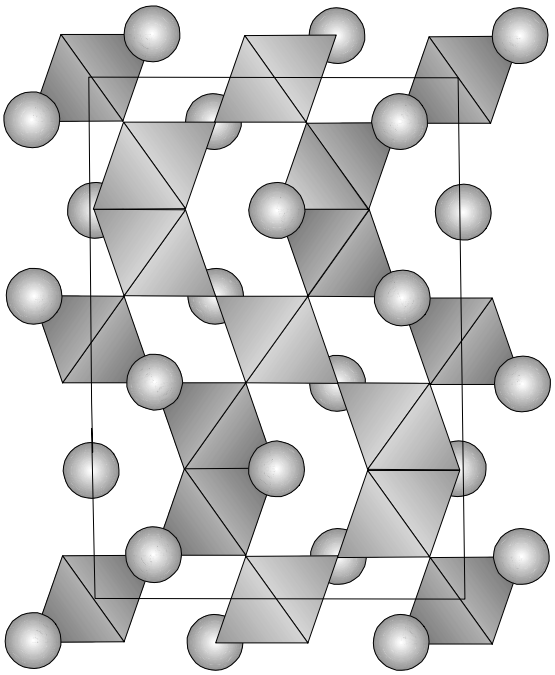

Hexagonal $BaTiO_3$ structure in the [110] projection. Octahedrons represent the TiO_6 coordination groups. In this view the close–packed sequence ABCACB is apparent.

The distance between idealized octahedral centers in the Ti_2O_9 groups is 0.234 nm however, the two Ti^{4+} ions (of the type Ti_{II}) brought together in these groups strongly repel each other and are consequently separated by the distance of 0.267 nm. With the presence of Ti_2O_9 coordination groups it should be possible for additional polymorphs of $BaTiO_3$ to exist, other than three–layer (Pm3m) and six–layer ($P6_3/mmc$) structures. However, there is no evidence for this in the scientific literature.

Literature Survey

In the last fifty years a lot of scientific literature on $BaTiO_3$ has been produced because of the material's importance to the electronics industry. Nevertheless, there are still several unsolved problems related to the local structure of twins in cubic $BaTiO_3$, their formation mechanism and the cubic–hexagonal transformation. A historical review given in this chapter provides an up–to–date information on these topics, and was used to delineate an own approach to the unsolved problems.

FIGURE 5

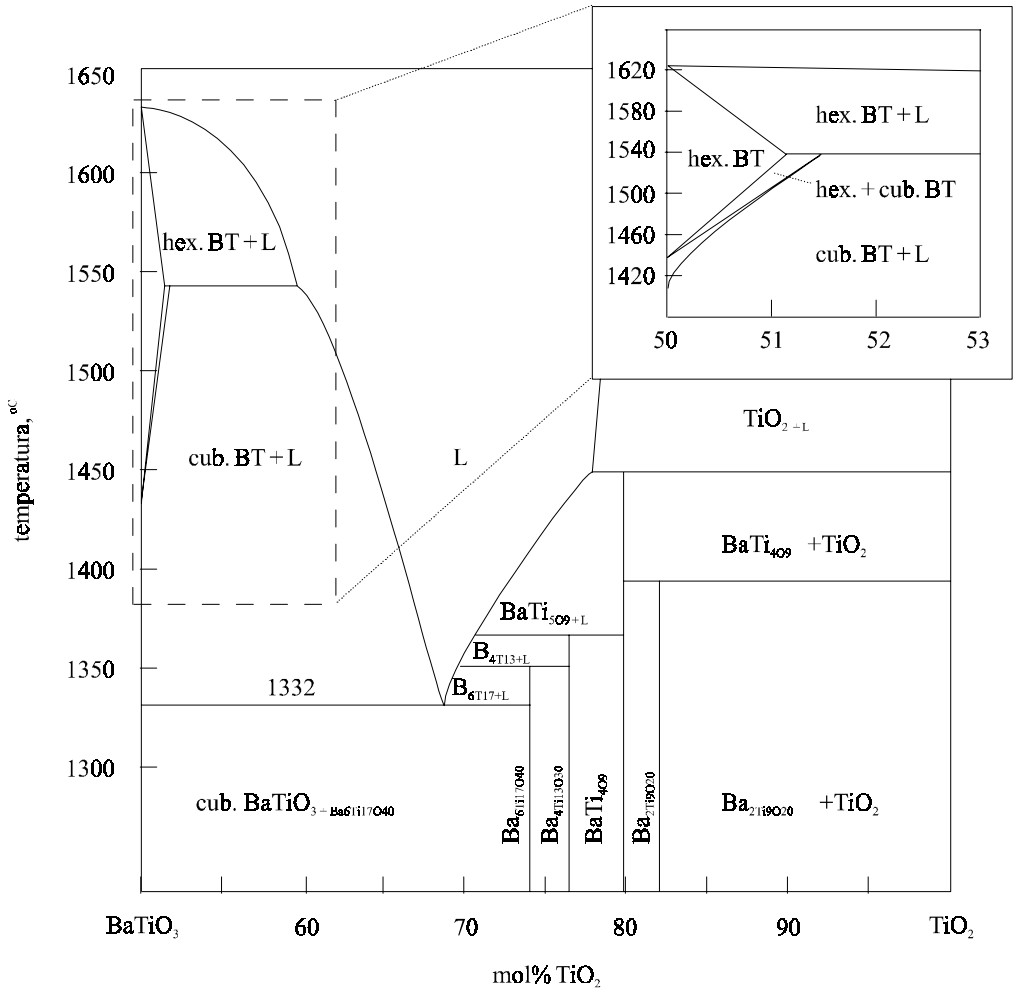

$BaTiO_3$–TiO_2 equilibrium phase diagram. Composition is given in the terms of the components $BaTiO_3$ and TiO_2. A detail in the upper–right corner shows the cubic–hexagonal phase transition (Kirby and Wechsler 1991).[15]

Cubic–hexagonal phase transition in the $BaTiO_3$–TiO_2 system

$BaTiO_3$ exhibits a reversible cubic–hexagonal phase transition at 1432°C. $BaTiO_3$ is often contaminated with Sr, which raises the transition temperature by 100°C per one mol% of $SrTiO_3$ (Kirby and Wechsler).[15] Between 1432 and 1539°C, in excess of TiO_2, the cubic and hexagonal phases coexist. Under reducing sintering conditions the transition temperature can drop by as much as 100°C and however, Sr additions can still exert a net increase on this transition temperature (Glaister and Kay).[16]

$Ba_6Ti_{17}O_{40}$ is the first compound that forms in the presence of small excess of TiO_2. Above the eutectic temperature $Ba_6Ti_{17}O_{40}$ is liquid and plays an important role in mass transfer during sintering. Its structure comprises a three–dimensional framework of TiO_6 octahedra sharing corners, edges and faces (Tillmanns and Baur);[17] the voids in this framework are filled with Ba. Under reducing sintering conditions this structure undergoes severe changes: oxygen loss is accompanied by the reduction of Ti^{4+} ions to Ti^{3+} (Bast et al. 1984).[18]

Other compounds from this phase system do not appear in the composition range investigated in this study. The following subsections are dedicated to the structural phenomena (structure and nucleation of {111} twins, cubic–hexagonal transition) that take place in pure $BaTiO_3$ sintered with small additions of TiO_2.

Structural models of the (111) twin boundary in $BaTiO_3$

In early structural studies it was found that the (111) twins do not form at elevated temperatures and pressures (Jugle 1966).[19] This fact appears to exclude a deformation mechanism for the formation of the twin. In addition, the reduction of the titanium ion had a marked effect on the propensity of a grain to twin. Grain growth under reducing sintering conditions resulted in a highly twinned microstructure.

A structural model for the coherent (111) twin, based on crystal chemistry, was proposed by Jugle.[19] The model consists of a hexagonal stacking fault, resulting in a face–sharing of two $[TiO_6]^{8-}$ octahedra to form $[Ti_2O_9]^{10-}$ groups at the twin boundary. The model is illustrated in Figure 6. Furthermore, Jugle suggested that the stacking at the twin boundary was more stable if highly polarizable Ti^{3+} ions were present in the $[Ti_2O_9]^{10-}$ groups. Such $[Ti_2O_9]^{10-}$ coordination groups had previously been proposed to build the structure of the hexagonal polymorph of $BaTiO_3$ (Burbank and Evans).[14]

FIGURE 6

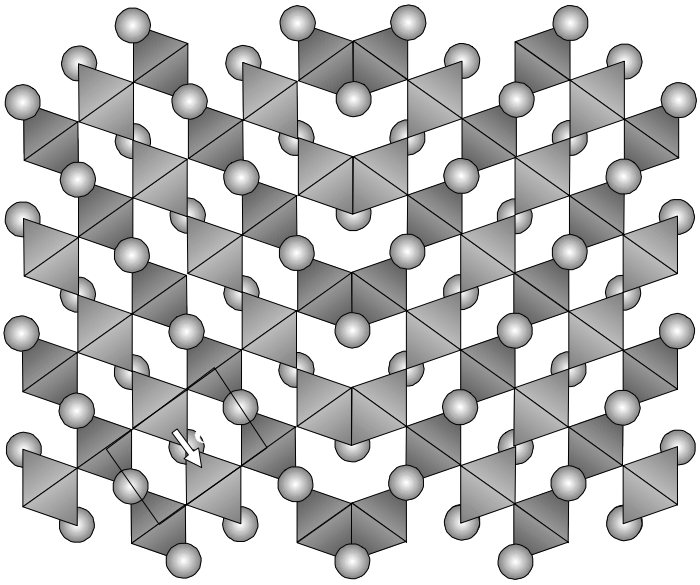

Schematic drawing of a coherent (111) twin in $BaTiO_3$, in the [1 1 0] projection, with a $Ba–O_3$ composition plane (Jugle 1966).[19] This model shows Ti_2O_9 coordination groups (similar to those found in the hexagonal polymorph) at the twin interface.

FIGURE 7

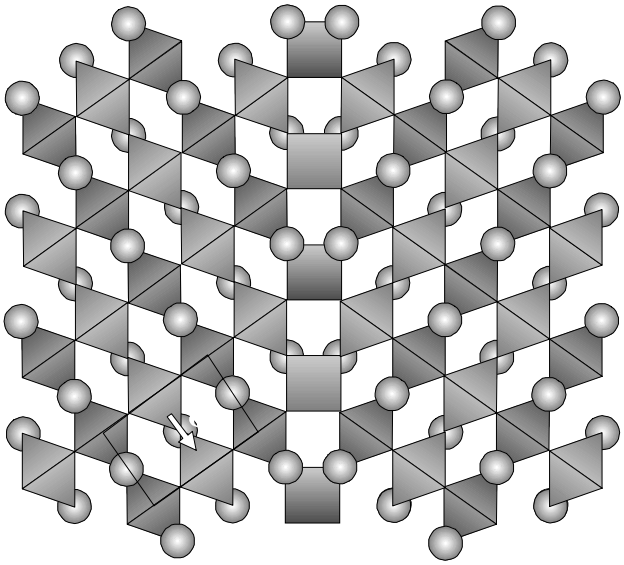

Schematic of a coherent (111) twin in $BaTiO_3$ in the [110] projection with a pure Ti composition plane (Eibl et al. 1988).[20] The fine octahedral coordination for Ti atoms is destroyed, instead a trigonal prism containing the Ti ion is formed at the interface.

In a high–temperature nonstoichiometric rutile (TiO_{2-x}), pairs of such face–sharing octahedra were also considered to be the most favourable sites for the accommodation of Ti^{3+} ions (Bursill et al. 1983).[21] Thus, oxygen loss is accompanied by the establishment of Ti^{3+} ions leading to the formation of face–shared octahedra. Oxygen vacancies would be mobile along the adjoining face.

In a crystallographic study of (111) twins in cubic $BaTiO_3$ by Eibl et al. (1988) [20] the atomic model of the twin boundary was discussed in terms of (Σ=3) coincidence site lattice unit cell. Accordingly, the interface plane consists of either Ba–O_3 (identical to that shown in Figure 6) or a pure Ti layer (shown in Figure 7). Crystallographically, the (111) twin would be formed on either plane by the same shear vector.

On the basis of an experimental high–resolution micrograph of the twin boundary, the authors provided evidence for a coherent twin and the absence of any intermediate phase. Considering the Aminoff and Broomé twinning rules (Cahn 1954) [22] and a short–range interaction for the two possible interfaces, Eibl et al. (1988) [20] preferred the Ba–O_3 plane as a coherent (111) twin interface in the cubic $BaTiO_3$. Using conventional TEM they showed that (111) twin in $BaTiO_3$ can be treated as a twin in the cubic phase.

FIGURE 8

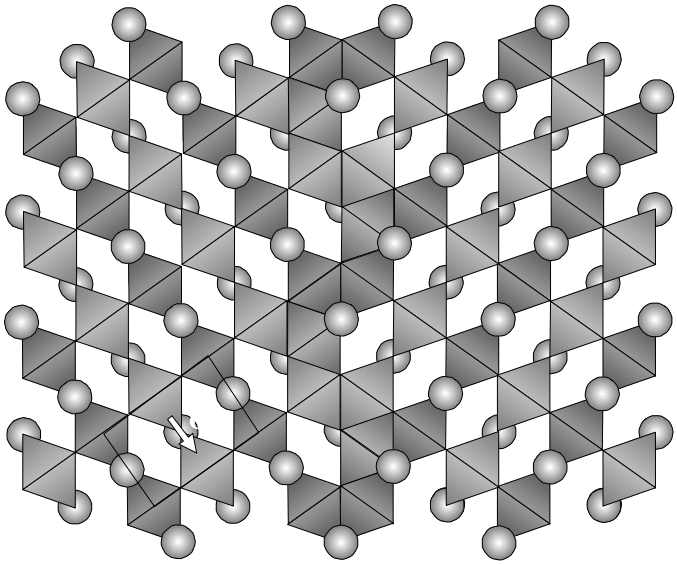

Schematic of a Ti–rich layer at the (111) twin in BaTiO3, shown in the [110] projection (Kraševec, Drofenik and Kolar 1990).[23] Note additional edge–sharing octahedrons at the interface. The octahedral coordination for Ti is preserved throughout the twin.

Kraševec, Drofenik and Kolar (1990) [23] proposed an atomic model for a so–called *non–conservative* (111) twin. The origin of twinning was explained on the basis of the structural similarity between the (111) layers of $BaTiO_3$ and (001) layers of the Ti–rich $Ba_6Ti_{17}O_{40}$ phase, that is always present when $BaTiO_3$ is sintered in an excess of TiO_2. The model comprises a thin precipitate of $Ba_6Ti_{17}O_{40}$ at the twin interface with a topotactic growth of $BaTiO_3$ on either side. This structure can be represented with two subsequent layers, where one is identical to that already proposed by Jugle,[19] and the other a Ti–rich layer having some extra TiO_6 octahedrons linked to the face–sharing octahedra by their edges. The proposed (111) twin structure is shown in Figure 8.

As support for their model they point to: (i) the topotactic relationship existing between $BaTiO_3$ and $Ba_6Ti_{17}O_{40}$ (Kraševec and Prodan 1983),[24] (ii) the composition range under which twins were observed to form which is conducive to the formation of $Ba_6Ti_{17}O_{40}$ and (iii) the likely presence of face–sharing octahedra at the twin boundary. On the basis of this model an explanation for anomalous grain growth was given.

Exaggerated grain growth and (111) twins

One of the possible causes for the exaggerated grain growth below the eutectic temperature is the presence of (111) twin boundaries in particular $BaTiO_3$ grains. The implications of the presence of anomalous grain growth below the eutectic temperature were first reported by Schmelz and Meyer (1982).[25] They observed that exaggeratedly grown grains contain these (111) twin boundaries. Their suggestion, that the occurrence of (111) twins strongly linked with exaggerated growth of these grains was supported by growth–mechanism investigation of Schmelz and Thomann (1984),[26] who pointed out the existence of two parallel (111) twins is a necessary condition for this anomalous growth, whereas grains containing only a single (111) twin boundary do not show abnormal coarsening. They also suggested that only *lamella–like* double twins have such a geometry which allows the crystal to grow without constraint in all six <211> directions. These sites have the highest growth rate at the so–called *re–entrant* angles of the (111) twins, and therefore grow in the form of pseudo–hexagonal platelets.

Growth mechanisms for such *lamella–like* twins have been studied extensively but the formation mechanism for these defects is not yet understood. The formation of the

(111) twins itself is, therefore, of a fundamental interest. The question arises as to during which of the processing steps these defects are most likely to form?

The first possible source of twinned grains is the calcination of the $BaCO_3$–TiO_2 powder, where $BaTiO_3$ forms by the release of CO_2.[1] Twins formed during this process are growth defects. The eagerness to solve a riddle of the formation of (111) twins led to some fairly speculative explanations as to their origin. In one of these studies, Kästner et al.[4] suggested, that twins form during the liquid–phase sintering. Accordingly, to their formation mechanism, $BaTiO_3$ grains undergo a coalescence in such a way that two grains come into the twinning orientation and then they couple into (111) twins. In a similar manner they extended their explanation to form multiple twin combinations. Needless to say that such a coalescence is very unlikely in a solid–state sintering processes and that for something like that to take place one would need flows of liquid phase, such as twin formation in feldspars in solidifying lava flows.

Despite all the effort put into these investigations the basic question remains unanswered, and moreover, unless the local structure and composition of the (111) twin is resolved there is no basis for further attempts to predict the formation mechanism.

The cubic–hexagonal transition under reducing sintering conditions

Sintering under reducing atmosphere lowers the cubic–hexagonal phase transition temperature by about 130 K (Glaister and Kay 1960).[16] A study of the influence of firing atmosphere on transition temperature (Wakamatsu et al. 1987) [27] showed that fractional conversion to hexagonal phase increases proportionally with increasing concentrations of reducing gases. Moreover, the quantity of Ti^{3+} was found to increase in proportion to with the amount of hexagonal phase. These observations suggest a substantial similarity between the formation of the widely studied hexagonal stacking at (111) twin boundary in cubic $BaTiO_3$ and the formation of the hexagonal polymorph itself.

Despite all this information, there is so far no indication in the literature that the growth mechanisms of double (111) twins in the cubic $BaTiO_3$ and growth mechanism of the hexagonal phase itself may in fact be identical.

Experimental Methods

Two types of materials were investigated. The first material was $BaTiO_3$ ceramic sintered below the eutectic temperature (formation of growth defects) and the second material was $BaTiO_3$ sintered above the eutectic temperature (formation of hexagonal polymorph). Both materials were prepared under reducing sintering conditions. The reducing atmosphere was employed to examine its influence on the formation of Ti_2O_9 coordination groups within the perovskite structure. Both types of sintered materials exhibit identical planar defects in cubic $BaTiO_3$ grains. For this investigation we mainly used materials prepared below eutectic temperature. Quantitative HRTEM with image simulation, was used to evaluate the previously mentioned atomic models and determine the atomic structure of the (111) twin boundary in cubic $BaTiO_3$. Spatially resolved EELS was used to study the oxidation state of Ti atoms along the (111) twin boundary. On the basis of these results, a new structural model for the coherent (111) twin in cubic $BaTiO_3$ which adequately describes the observed interfacial properties was proposed.

Sintering below the eutectic temperature

$BaTiO_3$ ceramic material was prepared by mixing high purity powders of $BaCO_3$ (Alfa 925700) and TiO_2 (Fluka AG 89490) in the molar ratio of 1:1.04. The powder mixture was calcined in an oxidising atmosphere for about four hours at 1080°C to produce $BaTiO_3$ with a release of the solid–state reaction product, CO_2. Calcined material was homogenised and pressed into thin pellets which were placed in an alumina crucible on a platinum foil and sintered in a laminar flow of a reducing gas mixture (10 mol% CO in N_2) at 1080°C for 2 hours. Subsequently, the temperature was then raised to 1250°C and held there for 4 hours to allow grain growth in the solid state.

Sintering above the eutectic temperature

$BaTiO_3$ ceramic was prepared by mixing high–purity $BaTiO_3$ powder (Transelco, code 219/9) with 2 mol% excess of $Ba_6Ti_{17}O_{40}$ powder. Homogenised powder mixture was pressed into thin pellets which were sintered for 1 hour at 1300°C and followed by an additional 10, 30, 60 and 240 minutes at 1400°C. The complete sintering process was performed in a laminar flow of a reducing gas mixture (8 mol% of H_2 in Ar). After sintering, the materials were cooled under reducing atmosphere to room temperature.

Experimental high–resolution transmission electron microscopy (HRTEM)

The sintered ceramic material was cut ultrasonically into 3 mm discs, which were mechanically thinned to an overall thickness of about 100 μm and subsequently dimpled to a thickness of 20 μm in the center. The TEM samples were produced by ion–milling with 6 kV Ar^+ ions until of the disc centre was perforated. This was followed by Ar ion–polishing at a glancing incidence of 4° to produce large, electron–transparent regions.

The HRTEM studies were performed using a high–resolution TEM microscope (JEM 4000EX) operated at an accelerating voltage of 400 kV. The microscope is equipped with a top–entry objective pole–piece (UHP 40H) having a point resolution of 0.17 nm and a small chromatic aberration. Other electron–optical parameters such as the convergence angle of illumination and the objective aperture size were determined from diffraction patterns. In the experimental work, grains close to a <110> projection were selected and tilted carefully into that zone axis.

FIGURE 9

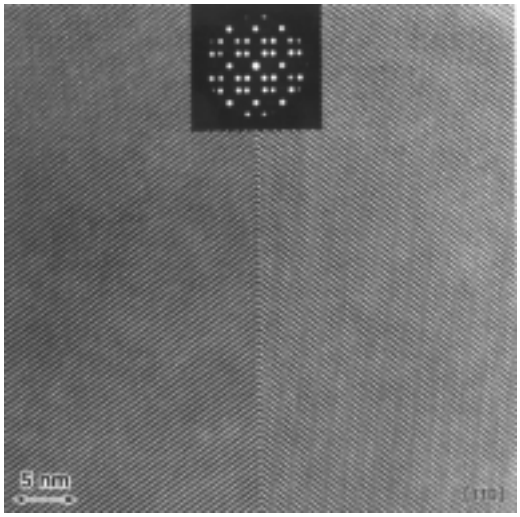

High–resolution image of the (111) twin boundary in BaTiO3 in [110] projection. Although accurately tilted into that zone axis lattice image shows obvious signs of some residual tilt at irregular intervals along the twin boundary.

Using a low–light–level camera attached to the microscope, images were recorded and then digitised. The online fast Fourier transform (FFT) of digitised images permitted rapid correction of the objective lens astigmatism. Residual beam tilt was reduced to

better than 0.2 mrad using *comma–free* alignment (Zemlin 1979).[28] Finally, micrographs were recorded under well defined defocus conditions. Actual defocus was determined by analysing optical diffractogramms from the negative plates, taken at the edge of the foil where amorphised material, produced by ion milling, is frequently present.

Acquiring an optimal tilt condition for a chosen zone axis at (111) twin boundary is a bit troublesome procedure. The main problem is that $BaTiO_3$ is tetragonal at room temperature. In the thin part of the crystal, where fine regions for experimental HRTEM may be found, domains do not form, and a residual stress, arising from a tetragonal transformation, that remains in the crystal is largely equalised by a deformation of the thin crystal foil. Thin crystal parts on each side of the twin boundary relax in different ways owing to their different orientation and geometry. This causes slightly misaligned [110] axes of the twinned crystals across the interface. Figure 9 on the previous page shows a typical high–resolution image of the (111) twin boundary in $BaTiO_3$.

A final tilting of the specimen in image mode using a small objective aperture, and by moving the zone of strongest scattering on both sides of the twin boundary to the thin crystal part, seems to be a very effective method for producing good lattice images. In fact, none of these images are really perfect since there is due to tetragonality always a degree of a residual zone–axis mismatch on either side of the twin boundary.

Experimental lattice images

In the TEM samples produced from materials prepared under reducing sintering conditions below the eutectic temperature, (111) twins were frequent. Approximately one in every three grains contained such a planar defect. During the course of this study, several twin boundaries oriented close to a <110> projection were investigated. For the same defocusing conditions and foil thicknesses lattice images of these defects exhibited a similar contrast behaviour. Moreover, the twins found in the samples from materials prepared above the eutectic temperature showed much the same behaviour, indicating that all the observed (111) twins are principally identical.

Experimental lattice images of a (111) twin boundary in $BaTiO_3$, viewed in [110] projection, are presented in Figure 10. All micrographs, although recorded for different imaging conditions, are from the same $BaTiO_3$ crystal. Images 10 (a) and (b) are taken

near Scherzer focus, whereas 10 (c) and (d) are closer to the first reverse passband of the contrast transfer function (CTF). Images 10 (c) and (d) appear somewhat different even though they were recorded under the same imaging conditions.

FIGURE 10

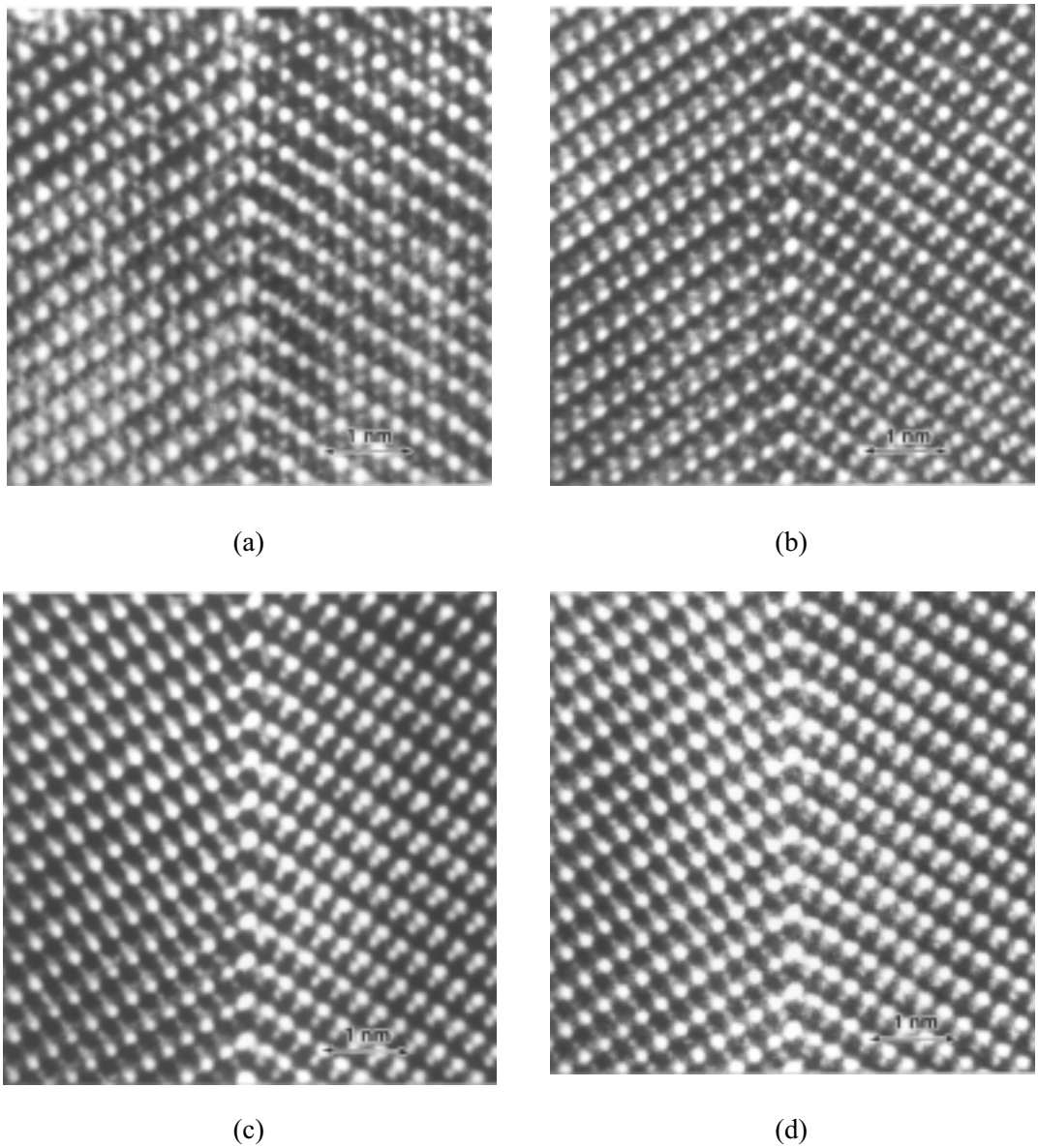

(a) (b)

(c) (d)

Experimental lattice images of the (111) twin boundary in BaTiO3 as seen in the [110] projection. Micrographs (**a**) and (**b**) are recorded near Scherzer focus, while (**c**) and (**d**) are closer to the first reverse passband of the CTF. Images (**b**), (**c**) and (**d**) are from a very thin region, whereas image (**a**) shows a thicker part of the crystal.

Determination of the imaging conditions

In order to determine individual atomic positions at the boundary on the basis of the HRTEM images, one must begin with reasonable estimates for matching simulated and experimental images for the bulk crystal. In Figure 11, optical diffractograms of the original micrographs, from which the images shown in Figure 10 were taken, are shown together with corresponding plots for the phase–contrast transfer functions. The CTFs are damped by the spatial and temporal coherence envelopes.

FIGURE 11

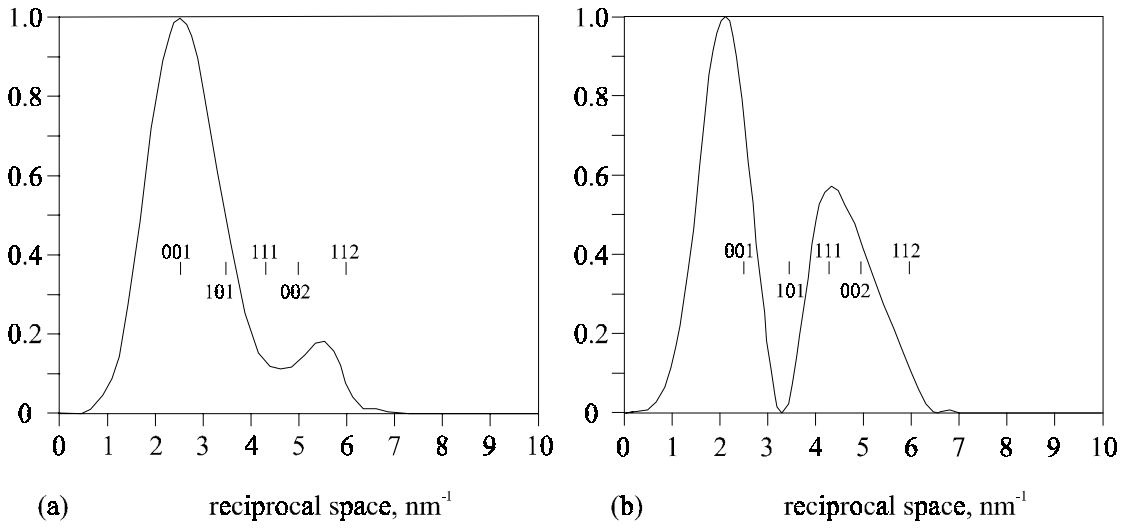

CTFs multiplied by spatial and temporal coherence envelopes for (**a**) 52 nm defocus with an inset of the diffractogramm corresponding to the lattice images in Figures 10 (a) and (b) and (**b**) 70 nm defocus with an inset corresponding to Figures 10 (c) and (d).

The diffractogram in Figure 11 (a) corresponds to the lattice images in Figures 3.10 (a) and (b), whereas that in Figure 11 (b) corresponds to the images in Figures 3.10 (c) and (d). The diffraction spots of a $BaTiO_3$ crystal were used to calibrate the length scale in the diffractogram. The calculated CTFs compared to the measured ones in Figure 11 indicate that the defocus value for the images in Figure 10 (a) and (b) is about –52 nm, and for Figure 10 (c) and (d) is about –72 nm. The accuracy of the actual focus settings, determined by this method, is estimated to be ±3 nm. On the basis of calculated defocus versus thickness tableau for $BaTiO_3$ in $[\bar{1}10]$ orientation the crystal thicknesses were estimated to be 6 nm for image 3.10 (a), and 4 nm for images 10 (b), (c) and (d).

Image simulations

In order to obtain detailed information on the atom positions, image simulations for the range of experimental imaging conditions were performed. These computations were performed by a multislice algorithm (EMS program package, Stadelmann 1987).[29]

FIGURE 12

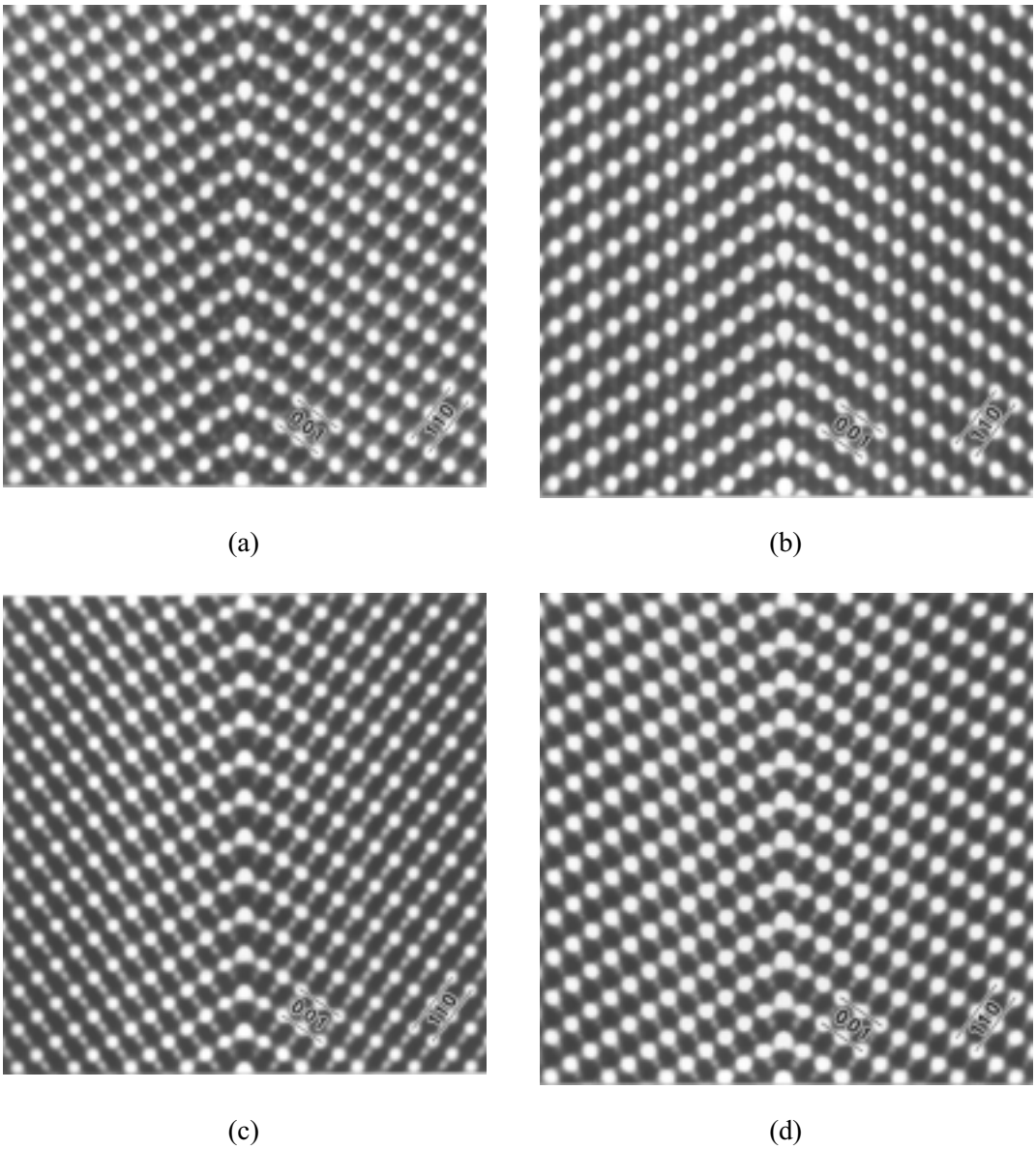

Filtered lattice images of the (111) twin boundary in BaTiO3 viewed in the [110] projection. Images (**a**), (**b**), (**c**) and (**d**) correspond to those in Figure 10.

Different structural models of the unrelaxed (111) twin boundary in the [110] projection were built into orthogonal super–cells with dimensions A = 4.166 nm, B = 0.986 nm and C = 0.565 nm. The plane of the defect was placed in the centre of the cell, parallel to the B axis, with the C direction parallel to the incident electron beam. The size of A was chosen to be large, to avoid boundary effects arising from the periodic continuation of the super–cell. Multislice computations employing dynamical scattering arrays of 512 x 128 beams were performed, resulting in a sampling resolution of about 0.008 nm along both the A and B translations. Following the electron–wave–field computation, image calculations were carried out for the electron–optical parameters of: a spherical aberration coefficient, C_s = 0.96 mm; focal spread, Δf = 8.0 nm; objective aperture size, D = 13.4 nm^{-1} and semi–angle of the beam convergence, Θ_c = 0.6 mrad.

The comparison between the experimental and simulated images was performed within a mathematical–graphic environment (IDL, Research Sys. Inc., Denver). For this purpose negative plates were digitised using a scanning camera (Eikonix 78/99) having a linear array of 2048 photodiodes with a 12–bit gray level. The noise from the digitized lattice images was reduced using an adaptive filtering method for periodic interfaces (Möbus et al. 1993).[30] The filtered experimental images are shown in Figure 12.

Simulated and filtered experimental images were compared and their grey levels were adjusted. Appropriate calculated images were finally scaled and inserted into the processed ones, which were then photographically reproduced from the screen.

Atomic model for the (111) twin boundary in $BaTiO_3$

Let us consider the lattice image in Figure 11 (c), recorded with a focus value near the first reverse passband and a thickness of about 4 nm ±1 nm. The image shows a coherent mirror twin in a <110> orientation. In this projection, columns consisting of Ba and O atoms in a bulk $BaTiO_3$ sample appear as strong white lozenges and the Ti atomic columns as slightly weaker dots in between, due to their smaller scattering potential.

For practically all imaging conditions, the pure oxygen columns do not cause a detectable contrast and the contrast of the Ba–O columns is mainly formed by the strongly scattering Ba atoms. Accordingly, the most pronounced features of the image in Figure 11 (c) match with the positions of the Ba–O columns. These strong contrast details, produced by the Ba–O columns in the bulk $BaTiO_3$, also appear in the boundary.

FIGURE 13

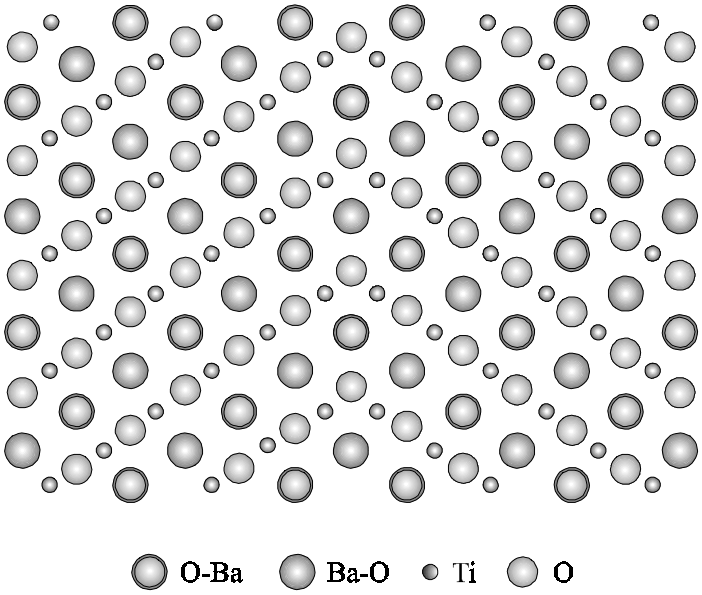

Unrelaxed structural model of the coherent (111) twin with a Ba–O_3 composition plane in the [110] projection. Atomic columns Ba–O, O–Ba, Ti and O are indicated. Note the Ti_2O_9 coordination groups at the interface.

By comparing the distances between the maxima in the intensity line scan over the boundary of the digitised lattice image it was found that the spacing between the (111) planes adjacent to the interface equals that of bulk $BaTiO_3$. The same result is obtained by overlaying the image containing the boundary onto the image of the bulk part of the crystal. Atomic displacements larger than 0.02 nm would be detected in this way. Using this information it is possible to construct an unrelaxed atomic model for the interface. A schematic drawing of a coherent (111) twin with Ba–O_3 composition plane in the [110] projection is shown in Figure 13.

Image simulations based on this model are inset into the images in Figure 14. In the lower part of the computed images Ba–O, O–Ba, Ti and O atomic columns are marked. Figure 14 (a) shows a simulated image for a thickness of 6.2 nm and a defocus of –54 nm together with the experimental micrograph of Figure 12 (a). Similarly, Figure 14 (b) is a region from Figure 12 (b) with a central inset showing an image simulation for a thickness of 4.0 nm and defocus value of –54 nm, whereas Figures 14 (c) and (d) correspond to those in Figures 12 (c) and (d) showing the computed insets for the 4.0 nm thickness and –72 nm defocus.

FIGURE 14

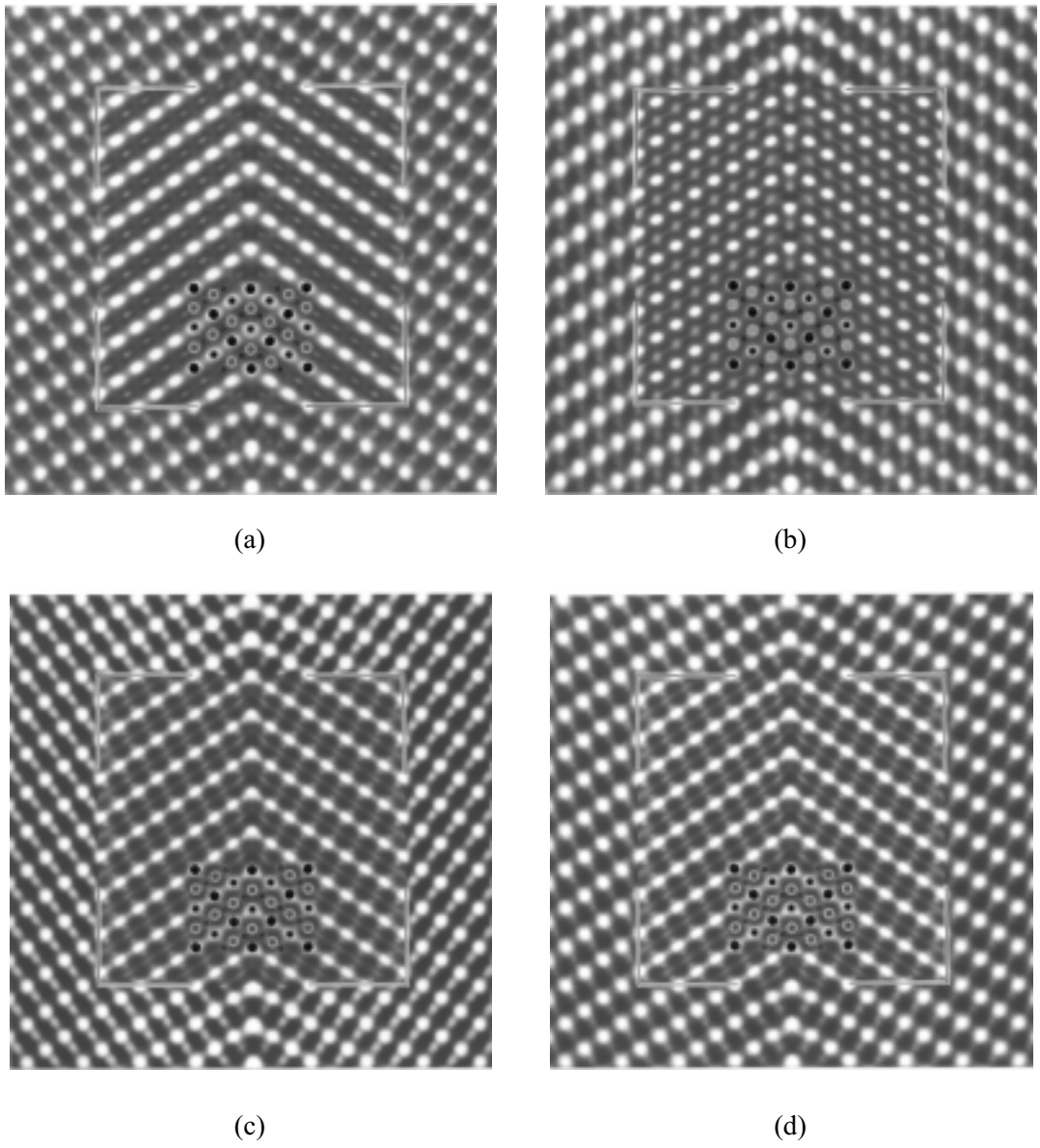

Simulated lattice images for the (111) twin, viewed in the [110] projection, inset onto the processed experimental images. Atomic columns Ba–O, O–Ba, Ti and O are marked in the lower part of the simulations. Images relate to those in Figure 12.

In Figure 14 (a) the interface is characterised by an array of intense white spots, separated by elongated black regions. In the simulation, one can recognise a small white dot lying below strong white spots. This corresponds to downwards–elongated intense white spot in the micrograph. In the bulk crystal stronger white spots are separated by

weak bright dots along [001] direction. The strong white spots in the bulk are somewhat weaker than those of the interface. The interface contrast in Figure 14 (b) bears a close resemblance to that in Figure 14 (a), but with the smaller dots slightly more distant from the strong white spots. This feature is more readily observed in the experimental image. In Figure 14 (b) white spots along the interface are separated by heart–shaped black regions. In the thinner crystal the strong white spots are separated by weaker ones along the [112] direction.

The 2–nm–thickness difference between Figure 14 (a) and Figure 14 (b) produces a significant difference in the contrast of the bulk. In Figures 14 (c) and (d) the interface contrast consists of intense white spots of Ba–O columns having blunted bottom sides. The Ba–O columns of the bulk crystal coincide with the strong white lozenges, whilst those of Ti coincide with weaker white dashes running along the [110] direction. In general, all the details of the experimental micrographs, particularly the ones from the very thin region, are successfully duplicated in the simulations.

Spatially resolved electron–energy–loss spectrometry

Spatially resolved electron–energy–loss spectra (SREELS) were recorded using a Gatan 666 parallel acquisition electron–energy–loss spectrometer (PEELS) fitted into a VG Microscopes HB501 dedicated scanning transmission electron microscope (STEM). The microscope was operated with only the second condenser lens excited and with the beam focused at the selected area aperture plane. The spectrometer collection angle, defined by the 2 mm entrance aperture, was 14 mrad semi–angle with an incident beam convergence semi–angle of 7 mrad. The estimated spectral resolution was 0.7 eV. The spectrometer dispersion was set to 0.2 eV/channel and calibrated employing the standard Gatan EL/P software. The Ti–edge position was determined by noting the extra voltage necessary to shift the inflection point of the edge threshold to the same channel previously occupied by the zero–loss peak. The inflection point of the oxygen K–edge threshold was measured to be 531 eV. The spectra consist of the sum of four photodiode readouts, each exposure being 30 s long.

The twin boundary was aligned parallel to the incident beam direction. To avoid multiple inelastic scattering only thin regions of the sample were examined. A set of

spectra was recorded with the beam scanning an area of 2 x 3 nm centered upon the twin plane, and a second set with the beam placed on the neighboring matrix. Smooth power–law fits were removed from the data. The spatial–difference spectrum was formed by subtracting a properly scaled matrix spectrum from that recorded at the boundary (Bruley 1993).[31] In this way spectral differences brought about by the presence of the twin plane become evident. This method automatically removes the photodiode readout pattern and minimizes the effects of channel–to–channel gain variation.

Chemistry of the (111) twin boundary in $BaTiO_3$

Considering the experimental observation, that these defects preferentially occur under reducing sintering conditions, one might expect, that the chemistry of the boundary plane would be affected. The formation of one oxygen vacancy in the $Ba–O_3$ composition plane would be accompanied by a change in the oxidation state of nearest neighbouring Ti atoms from Ti^{4+} to Ti^{3+} in order to retain the local charge balance.

In the idealised structural model for the coherent (111) twin Ti atoms along the twin boundary are in the oxidation state of Ti^{4+}. A modification of this model from $[Ti_2O_9]^{10–}$ for the composition of the face–sharing octahedra to $[Ti_2O_8O^{¨}]^{10–}$ would not significantly alter the image contrast, since an oxygen atom has a fairly low scattering potential, and the cation coordination is preserved. In order to study the possibility of a lowered oxidation state for the Ti ions at the twin boundary, EELS was employed. The near–edge structure of the Ti $L_{2,3}$ edge is known to be sensitive to the oxidation state, and chemical and structural environments of the Ti ions (Leapman et.al 1982;[32] Otten et al. 1985;[33] Sankararaman and Perry 1992;[34] Brydson 1991;[35] DeGroot et al. 1990 [36]).

Here, the use of the spatial–difference mode is used to reveal small changes in the energy–loss near–edge structure (ELNES) caused by the boundary. A spatial–difference spectrum exposes these changes by removing the energy dependant background. Spectra recorded at the boundary and about 4 nm away from it on both sides (assigned as upper and lower) are illustrated in Figure 15. The general shapes of the Ti $L_{2,3}$ edge and the O–K edge are not that significantly different from previously published data. The Ti edge structure is dominated by the spin–orbit split L_3+L_2 white lines which are due to transitions from $2p_{3/2}$ and $2p_{1/2}$ to unoccupied d orbitals peaking at about 461 eV and 466 eV. The inflection point of the edge threshold was located at 458.5 eV.

FIGURE 15

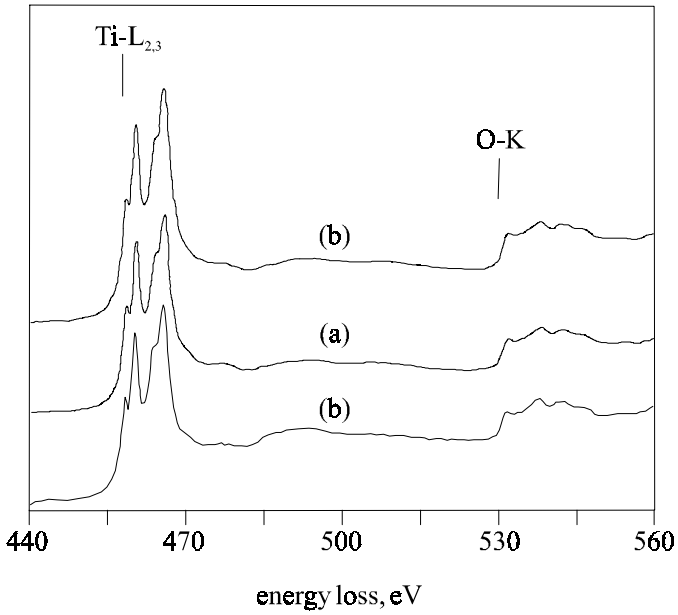

The Ti $L_{2,3}$ ond O–K edges recorded (**a**) on the twin boundary and from (**b**) both sides of the bulk $BaTiO_3$ crystal, about 4 nm away from the interface. There are no obvious compositional differences.

FIGURE 16

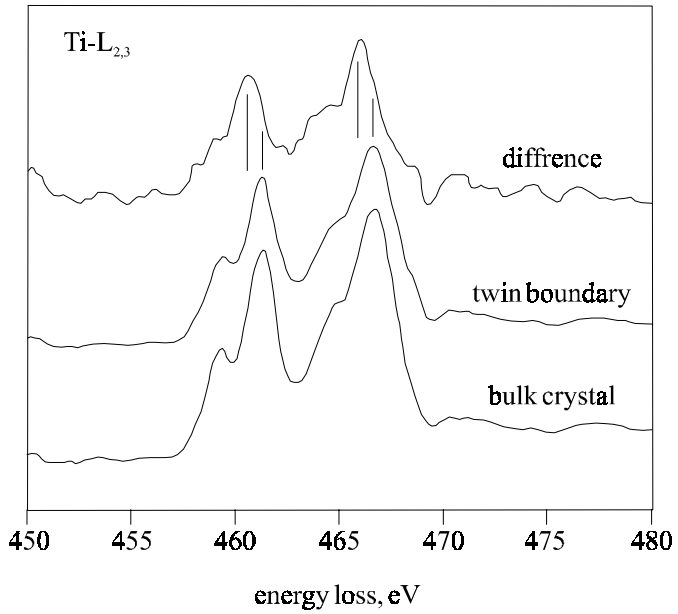

Close up of $Ti_{2,3}$ edges. The difference spectrum (the twin boundary spectrum minus scaled matrix) is shifted to a lower energy relative to the bulk crystal by 0.7 eV. Its intensity is about 10 % of the original spectrum.[37]

A further splitting of the Ti L_2 and L_3 components is due to the crystal–field effect on the $2t_{2g}$ (at 459.4 eV) and $3e_g$ (at 461.3 eV) molecular orbitals in the octahedral symmetry. This is more clearly seen in Figure 16. The ELNES of the bulk $BaTiO_3$ phase is compared with the spatial–difference spectrum which exhibits the same structure but is shifted towards lower energy–loss by ~0.7 eV. Both the spin–orbit splitting between the L_2 and L_3 edge, and the L_3/L_2 intensity ratio do not change significantly, this value is about 0.8. The absolute intensity of the difference spectrum is about 10 % that of the matrix spectrum. This is consistent with about one monolayer of affected Ti ions and is similar to the value of 0.8 reported by Leapman et al. (1982).[32]

FIGURE 17

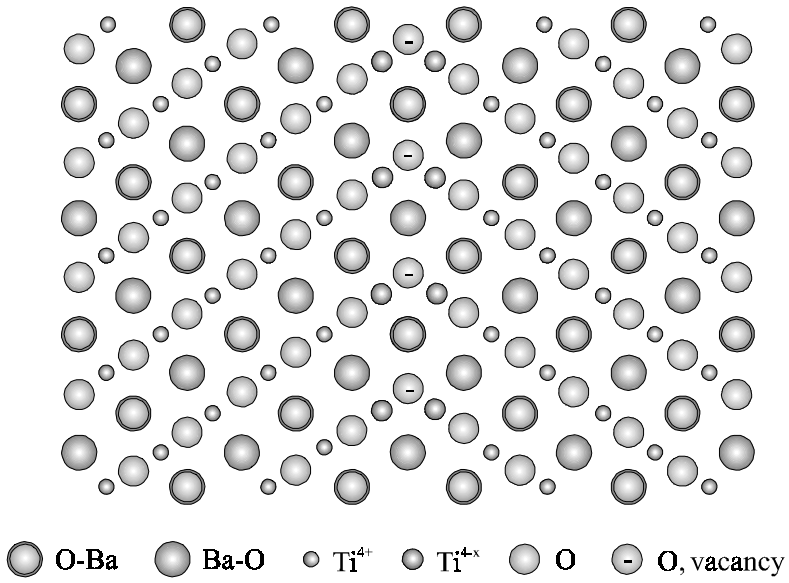

A modified structural model of the (111) twin interface, showing positions of Ti^{4-x} ions along the boundary. The composition of the boundary plane is $Ba–O_{3-x}[O^{¨}]_x$ instead of the Ba–O_3 and that of face–sharing octahedra $[(Ti^{4-x})_2O_{9-x}(O^{¨})_x]^{10-}$ instead of $[Ti_2O_9]^{10-}$.

The most attractive explanation for the observed downward shift at the interface is a reduction in the Ti oxidation state at the twin plane. A modified structural model for the oxygen–deficient (111) twin boundary is shown in Figure 17. This model preserves the octahedral coordination and incorporates oxygen vacancies in the interface plane with the Ti ions along that plane with an oxidation state lower than 4+.

Atomic Structure of the (111) Twin Boundary in Barium Titanate

The coherent (111) twin boundary in $BaTiO_3$ was investigated using quantitative HRTEM and spatially–resolved EELS methods. Lattice images under different focusing conditions were obtained and compared to simulated images for different structural models. An excellent match between calculated and observed images was obtained only for the model where Ba–O_3 plane constitutes the twin boundary (Rečnik et al. 1994).[38] The oxidation state of Ti at twin boundaries was interrogated by studying the near–edge structure of the L_{23} ionisation edge of Ti using spatially resolved EELS (Bruley et al. 1993).[37] The difference between the bulk and boundary spectrum indicates the presence of Ti in a reduced oxidation state at the boundary. The charge is compensated by oxygen vacancies, $O^{¨}$ in the twin plane, then composed of Ba–$O_{3-x}[O^{¨}]_x$ instead of Ba–O_3.

Composition of the (111) twin boundary in $BaTiO_3$

By resolving the atomic structure of the coherent (111) twin boundary in $BaTiO_3$ it was shown that a Ba–O_3 layer constitutes the composition plane. This observation is in accordance with the suggestions of the previous authors (Jugle 1966;[19] Eibl et al. 1988;[20] Kraševec et al. 1990 [23]). The three structural models for (111) twin: (i) Judgle's model,[19] based on crystallographic considerations, (ii) Eibl's first model,[20] based on Aminoff and Broomé's rules [22] of twinning and (iii) our model, based on the quantitative HRTEM analysis, are in essence the same. In the model where the (111) twin boundary consists of a Ba–O_3 layer and the $[TiO_6]^{8-}$ octahedrons along the composition plane share faces, the interfacial structure is the same as that found in the hexagonal polymorph of $BaTiO_3$. $[Ti_2O_9]^{10-}$ groups are elementary parts of the (111) twin and the octahedral coordination of Ti, typical for Ti–O compounds, remains preserved throughout the twin structure. The close similarity between the interfacial structure of the (111) twin and the hexagonal phase of $BaTiO_3$ may play an important role in cubic–hexagonal transition mechanism.

Other structural models, suggested in the literature by Eibl et al.[20] and Kraševec et al.[23] were also tested by our image simulations, but they do not resemble the observed images. In particular, the model suggested by Eibl et al. (1988),[20] where a pure Ti layer constitutes the boundary plane, does not apply to any of the experimental lattice images and can therefore be rejected. In addition, no intermediate polytypoidic phase, such as

$Ba_6Ti_{17}O_{40}$, could be observed at the (111) twin interface in any of the specimens investigated. This is in agreement with the observations of Eibl et al.[20] Therefore, we found no experimental evidence, so far, for the existence of the non–conservative twins postulated by Kraševec et al.[23]

Atomic relaxations due to the repulsion of the Ti^{4+} ions in the $[Ti_2O_9]^{10-}$ groups, as expected by Eibl et al.[20] could not be detected on the experimental images. There may exist relaxations, however, the shifts normal to the boundary plane do not exceed 0.02 nm or else they would have been visualised. This means that the Ti–Ti bond length of 0.267 nm in $[Ti_2O_9]^{10-}$ of hexagonal $BaTiO_3$ as reported by Burbank and Evans (1948) [14] does not apply for the Ti–Ti bond length in $[Ti_2O_9]^{10-}$ at the (111) twin interface. The actual Ti–Ti distance across the interface may be in the range of ±0.02 nm around the value of 0.234 nm for the unrelaxed twin boundary. This discrepancy between the Ti–Ti bond lengths could be accounted for if the Ti in the face–sharing octahedra at the interface had a lower oxidation state such as Ti^{3+}.

In this way a short–range electrostatic repulsion is reduced giving a rise to shorter bond lengths than in the hexagonal polymorph. In order to balance the charge oxygen vacancies $O^{\cdot\cdot}$ would be needed in the twin plane. In the extreme case, where all of the Ti ions along the boundary plane are replaced by Ti^{3+} in the $[Ti_2O_9]^{10-}$ groups it would become $[Ti_2O_8O^{\cdot\cdot}]^{10-}$. The octahedral coordination of the Ti ions in these groups remains preserved. Such a stoichiometric deviation in the boundary composition is a strong indication for (111) twins in $BaTiO_3$ to be formed as growth defects under reducing sintering conditions (Rečnik and Kolar 1993).[39]

Reduced state of the (111) twin interface

There are a number of factors that may contribute to the observed chemical shifts. These include core–level shifts due to a charge transfer, modifications to the valence conduction–band density of states and the changes in the many–electron interactions. According to Leapman et al. (1982),[32] there is a 1.4 eV chemical shift between metallic Ti^0 and oxidized Ti^{4+} in TiO_2, measured by EELS. The difference was attributed to the development of the bandgap in TiO_2, the core–hole excitonic interaction and many–electron adiabatic relaxation mechanisms. XPS measurements indicate a 4.9 eV core–level shift for the four electron valence state (Ramqvist et al. 1969).[40]

In $BaTiO_3$, the Ti atoms along the twin interface are expected to occupy similar environments to the bulk, and therefore one would not expect gross differences in the electronic structure. Scaling to either the EELS by Leapman el al. [32] or the XPS data of Ramqvist et al.[40] one might anticipate a chemical shift between 0.3 and 1.2 eV for a single electron valency change. The measured 0.7 eV shift falls within this range supporting the notion that the interface Ti layers are occupied by titanium ions having a lower oxidation state than those of the bulk $BaTiO_3$.

Other EELS analyses of various Ti oxides by Otten et al.[33] and Sankararaman et al.[34] having worse energy resolution, as evidenced by the unresolved crystal field splittings, both indicate a 2 eV shift between the Ti^{4+} and Ti^{3+} oxidation states. The chemical shift on the (111) twin boundary in barium titanate is smaller and therefore may reflect some intermediate oxidation or a degree of covalency.

The formation Mechanism of Growth Twins in $BaTiO_3$

The stoichiometric deviation in the boundary composition, as shown by EELS measurements in the previous section, strongly suggest that the (111) twins in $BaTiO_3$ are formed as growth defects. Growth twins were observed in materials prepared either below or above the eutectic temperature, however, the structure and composition were only determined for the twins found in materials prepared without the presence of liquid phase. A possible growth mechanism is discussed in terms of the preparation conditions under which these defects form, combined with the information about their structural and compositional properties. A possible nucleation mechanism is proposed that appears to explain the nature of these defects most adequately. In addition to (111)–type twins, (112)–type twins have also been encountered during the course of this study.

Observed (111) twin combinations

The most common growth defects observed in the investigated materials are single (111) twins. These defects sometimes appear in pairs. Three elementary combinations of (111)–type twins are found, and Figure 18 illustrates the three possible (111) twinning associations encountered in $BaTiO_3$.

FIGURE 18

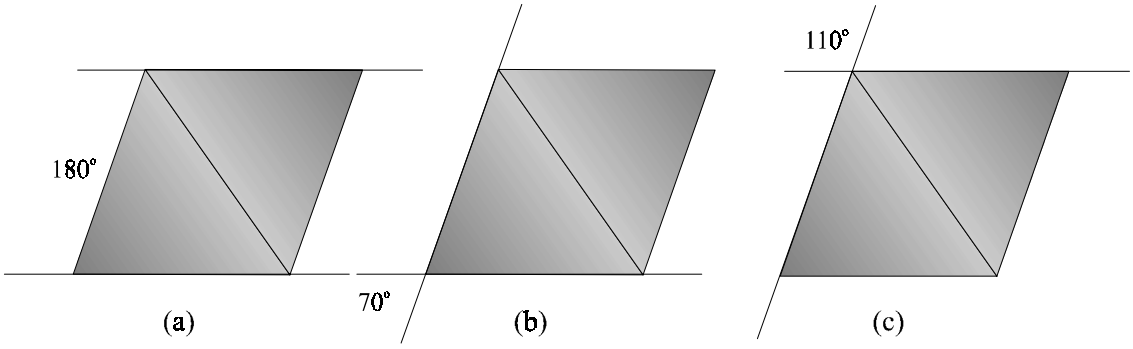

The three possible (111) twin combinations found in $BaTiO_3$: (**a**) parallel or 180°, (**b**) acute or 70° and (**c**) obtuse or 110° twin combination.

FIGURE 19

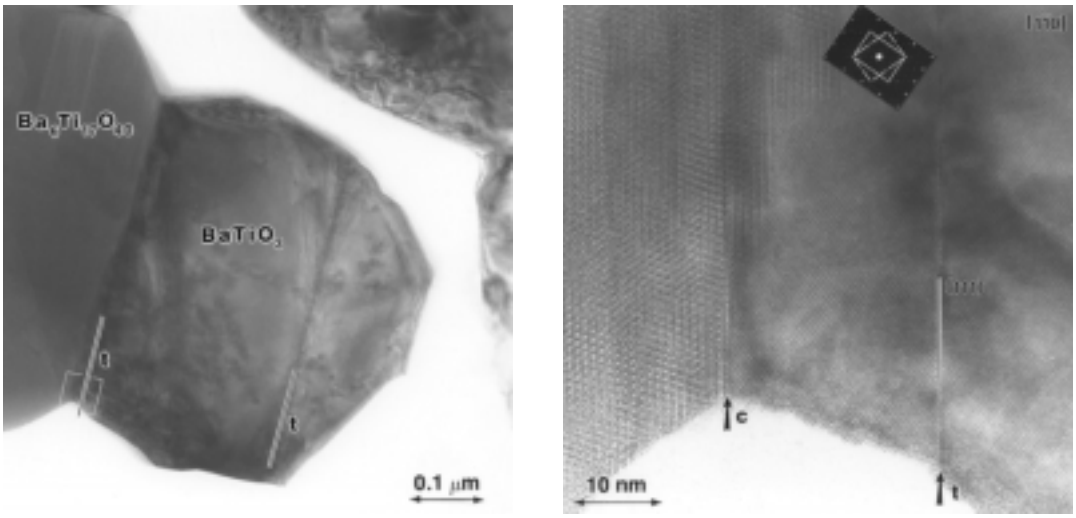

(a) (b)

(**a**) TEM micrograph of a parallel (111) twin combination. In the vicinity of the leftmost twin boundary the $BaTiO_3$ grain is intergrown with a $Ba_6Ti_{17}O_{40}$ grain . This appears to be the best example found in these materials which supports the hypothesis of the twin structure including a Ti–rich phase at the interface (Kraševec et al. 1990).

(**b**) HRTEM image of the region marked in (a) clearly shows no intermediate phase at the twin boundary, marked with **t**. The Ti–rich phase is far distant from the (111) twin interface, the interface between $BaTiO_3$ and $Ba_6Ti_{17}O_{40}$ is marked with **c**. the diffraction pattern of the boundary region shows overlapping information from both crystals.

FIGURE 20

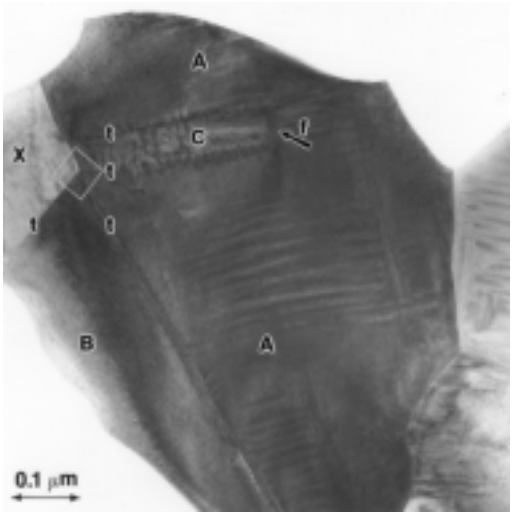

(a)

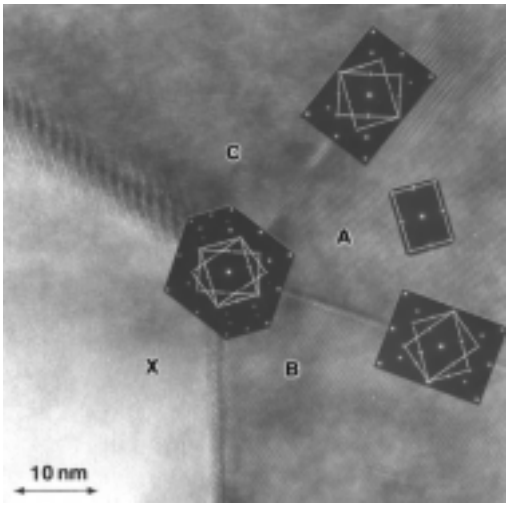

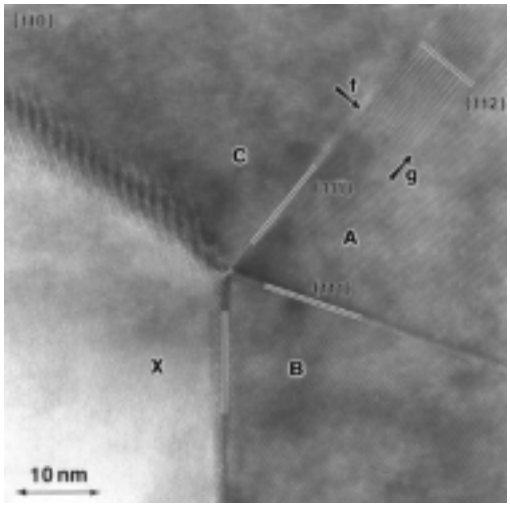

(b) (c)

(**a**) TEM micrograph showing a rare acute angle combination of (111) twins. What makes this grain unusual is that it contains not only the acute pair of twins, but also a parallel twin combination ending within the grain with a perpendicular planar defect marked with **f**. The junction point of the acute pair is enlarged in (b) and (c).

(**b**) and (**c**) HRTEM image of the junction point showing a complex diffraction pattern, that is a sum of the twin patterns arising from boundaries C|A and A|B. In addition to these B|X also seems to be a twin, with the crystal X out of the zone axis. On the C|A boundary **g** denotes a (111) twin and **f** a gliding (112) twin showing a Mioré pattern.

These are: (i) a *parallel* or 180° twin combination, enclosed by (111) and $(\bar{1}\bar{1}\bar{1})$ planes, with the width of the platelet between 50–200 nm; (ii) an *acute* or 70° twin combination, enclosed by the (111) and $(11\bar{1})$ planes; and (iii) an *obtuse* or 110° twin, enclosed by (111) and $(\bar{1}\bar{1}1)$ planes; all indexed for the $[\bar{1}10]$ projection. Surprisingly, the geometry of the observed (111) twin combinations appears to be closely related to the geometry of an octahedron. This implies that the origin of coupled twins lies in the morphology of the original $BaTiO_3$ crystallite. The most common is the *parallel* twin.

FIGURE 21

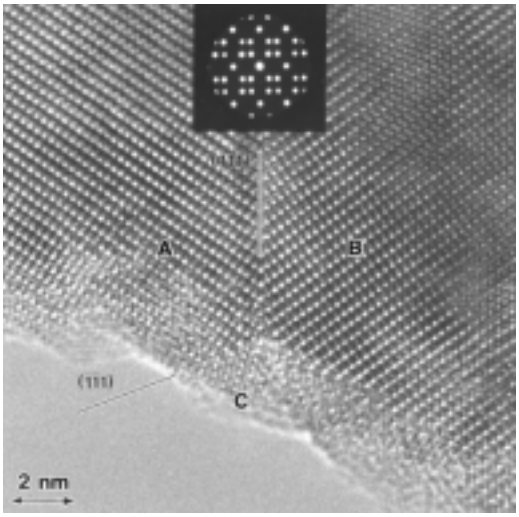

HRTEM image of the (111) twin boundary A|B. The amorphous $BaTiO_3$ material at the edge of a thin crystalline region crystallizes under the influence of the electron beam. This phenomenon complicates the alignment since a disappearing amorphous material disables a rapid objective astigmatism corrections, but it often results in the formation of (111) twins on the crystal edge. This indicates, that the environment in the microscope is similar to the sintering under reducing conditions. In this way a (111) twin was formed on the edge of crystal A producing the obtuse twin combination, where the angle between A|B and A|C twins is in fact 110°.

Nucleation of the (111) twin in $BaTiO_3$

By considering the experimental conditions under which (111) twins form, the three possible growth combinations of individual (111) twins, and taking into account the structural and compositional properties of such a defect, a possible formation mechanism is proposed. In samples sintered below the eutectic temperature with the reducing atmosphere introduced below 1100°C, there is an abundance of (111) twins.

About one in every three grains contained such a planar defect. In contrast, hardly any twins are found in materials sintered using the same temperature regime, but with the reducing atmosphere introduced at 1250°C. This is a strong indication that the reducing conditions play an important role at a very early stage of the sintering.

At this stage, the exposed octahedral faces of the crystallites in the initial $BaTiO_3$ powder undergo a reduction process. An equilibrium quantity of oxygen from the $Ba–O_3$ close–packed surface layer of the {111} planes is removed. An oxygen deficient $Ba–O_2O^{¨}$ layer is an obstruction to the normal growth of $BaTiO_3$ grains. However the charge compensation by reduction of the neighbouring Ti layers from its normal Ti^{4+} to the Ti^{3+} oxidation state results in the formation of face–sharing $Ti_2O_8O^{¨}$ coordination groups. These groups are, according to a structural and spectroscopic investigation by Rečnik et al. (1994),[38] elementary parts of the (111) twin boundary.

At higher temperatures when the diffusion in the solid state occurs, the material deposited on such surfaces grows because of the faulted surface structure in the only possible – twinning orientation with respect to the original $BaTiO_3$ crystal. In this way, single twins, or any of the three twin combinations described above form.

It is important to note that the proposed formation mechanism may not be the only source of twinned crystals. Depending on the preparation method, twins are, to a certain extent, present in the $BaTiO_3$ powder (Eibl et al. 1987).[1] If such a crystal undergoes the process described above, more complex twin combinations may be observed, for example see Figure 20.

Experimental evidence for the existence of (112) twins in $BaTO_3$

Occasionally (111) twins end within the grain with a step–forming perpendicular defect. The nature of this planar defect indicates a (112)–type twin. High–resolution images of a step–forming combination of $(11\bar{1})$ and (112) twins are shown in Figure 22. The twins grew under the electron beam in the electron microscope. (112) twins also appear in sintered materials, although they are very rare and so difficult to find in a thin crystalline region convenient for HRTEM. Such a case is shown in Figure 20 (a) where *parallel* (111) twins end within the grain with a (112) twin.

FIGURE 22

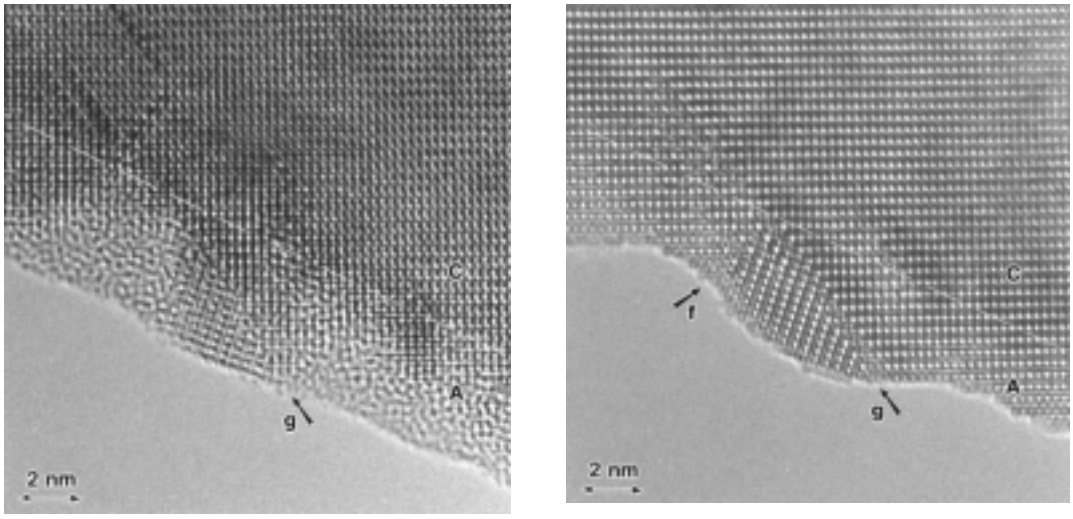

(a) (b)

(**a**) HRTEM image showing an early stage of (111) twin growth from the amorphous $BaTiO_3$ material present on the crystal edge, in a similar way to that in Figure 21. A white dashed line indicates the approximate position of the crystalline–amorphous boundary C|A before heating the region with the high–energy electrons. The marker **g** points in the direction of an already nucleated (111) twin. A lack of the amorphous material in the vicinity of the twin implies, that the twin grows at a higher rate than the remainder of the $BaTiO_3$ crystal. Note, that the amorphous edge is originally parallel to the C|A boundary.

(**b**) HRTEM image showing the end stage of (111) twin growth. The (111) twin, marked with **g**, is now completely developed. It consumed all the amorphous material from its neighbourhood, becoming thick in comparison with the rest of $BaTiO_3$ crystal, relative to the original A|C boundary. However, the new twin boundary could not invert the existing $BaTiO_3$ crystal into a twin, and had to end with a perpendicular (112)–type twin. A (112) twin always appears in a combination with the (111) twin, and is never observed as an isolated defect. Therefore, (112) twins are growth–enforced twins.

Cubic (111) Twins and Hexagonal $BaTiO_3$

The influence of reducing sintering conditions on the anisotropic grain growth in $BaTiO_3$ above the eutectic temperature was investigated. The morphology and structure of exaggeratedly grown grains were examined by XRD, SEM and HRTEM. The results showed that all the exaggeratedly grown grains were hexagonal $BaTiO_3$ in the form of platelike crystals with *a*:*c* ratios up to 10. In addition, it was found that the direction of exaggerated growth of the parallel (111) twins in a cubic phase was crystallographically equivalent to the direction of exaggerated growth of the hexagonal phase. The reducing

atmosphere during the sintering process was thought to trigger a reduction of Ti^{4+} to Ti^{3+} which plays an important role in the formation of hexagonal stacking.

Powder XRD was used to study the cubic–hexagonal transformation in $BaTiO_3$. The morphology of hexagonal grains was investigated by SEM and finally, to check for the presence of a liquid phase and to ascertain the crystallographic direction of the exaggerated growth, TEM was used. On the basis of the results and the close similarity between a phenomenon of exaggerated growth of *parallel* (111) twins below the eutectic temperature and that of hexagonal phase above the eutectic temperature, a model for the exaggerated growth of hexagonal $BaTiO_3$ in the presence of a liquid phase is proposed.

Examination of crystal morphology using scanning electron microscopy

The morphology of anomalously grown grains was examined in polished cross–sections and on the surfaces of the pellets, using Jeol 840 scanning electron microscope.

From cross–section micrographs one would expect either a rod–like or plate–like morphology for the anomalously grown grains. Three–dimensional information can be obtained from the surface of the sintered ceramic where the crystals develop without any restraint. Single crystals of cubic $BaTiO_3$ and some twinned grains, are shown in Figure 23, and plate–like hexagonal crystals are shown in Figure 24, within the matrix of glassy liquid phase. Images 23 and 24 show typical surface microstructures of these materials.

The morphology of the anisotropic hexagonal crystals does not show a six–fold axis along the basal plane (001) which would be expected for the 6/mmm symmetry. Different central distances of the {101} and $\{10\bar{1}\}$ faces imply a trigonal symmetry, such as 3m, rather than the hexagonal 6/mmm where the {101}–type faces would have been equally developed. An explanation for such a morphology may originate in a distorted hexagonal symmetry, resulting from a change in the oxidation state for the Ti ions and the formation of $O^{\cdot\cdot}$ vacancies as a result of the reducing sintering conditions.

FIGURE 23

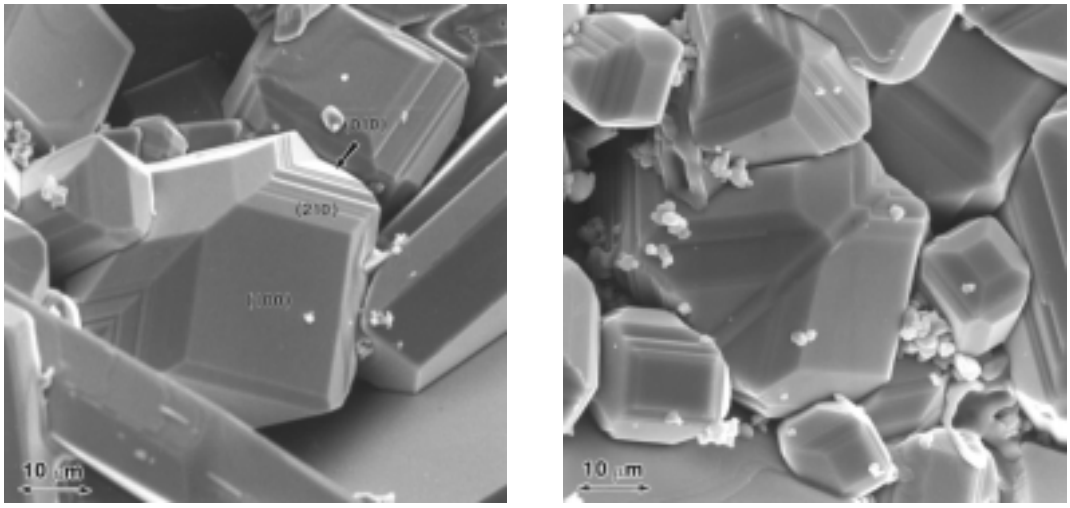

(a) (b)

(**a**) SEM micrograph showing a (111) cubic twin with well–developed {100} and {210} faces. Occasionally cubic crystals also exhibit the {110} and {111} forms.

(**b**) SEM micrograph of triple parallel (111) twins. Double parallel twins also occur in these materials appearing as faulted single crystals parallel to the twinning (111) plane.

A schematic drawing of the observed crystals compared to the morphology of the true hexagonal crystals is shown in Figure 25. Taking a closer look at the basal plane of such a hexagonal platelet, shown on Figure 24 (a), we can recognise surf–shaped figures formed by vicinal faces. Such faces form preferentially due to the lattice imperfections which may be caused by the presence of inclusions or accidental crystal interfaces, or in the direction of a higher growth rate (Rečnik and Kolar 1996;[41] Kolar et al. 1998 [42]).

Three types of crystalline inclusions are found by EDX in hexagonal $BaTiO_3$ crystals: (i) cubic $BaTiO_3$ grains in the form of single crystals or (111) twins, (ii) liquid phase inclusions with a composition close to $Ba_6Ti_{17}O_{40}$ and, in some rare cases (iii) needle–like rutile inclusions. None of these seem to be in any explicit crystallographic relationship with the hexagonal $BaTiO_3$. The amount of (111) twins in the cubic phase is relatively high in these materials. Combinations of double and even triple *parallel* (111)

FIGURE 24

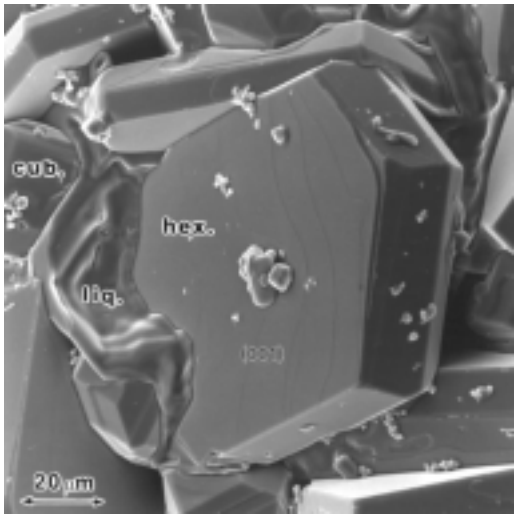

(a)

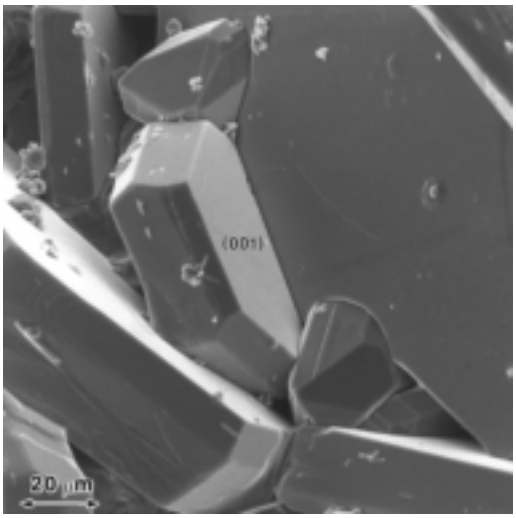

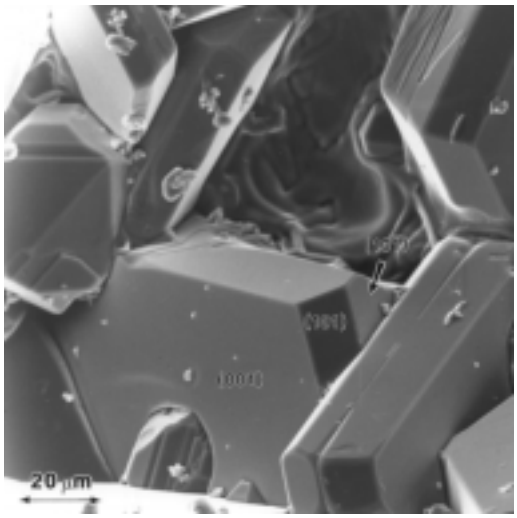

(b) (c)

(**a**) SEM micrograph of a hexagonal $BaTiO_3$ crystal, grown on the surface of the pellet, with extremely developed {001} faces. Vicinal forms on the {001} facets indicate a high mass transport from the liquid phase in the direction of a higher growth rate,i.e. <100>.

(**b**) and (**c**) SEM micrographs, showing the loss of a six–fold symmetry along the basal plane. Differently developed pyramidal faces indicate a trigonal symmetry. This observation implies atomic displacements in the hexagonal structure.

twins are found. These twins do not show any exaggerated growth as they would below the eutectic temperature where no hexagonal phase is present.

FIGURE 25

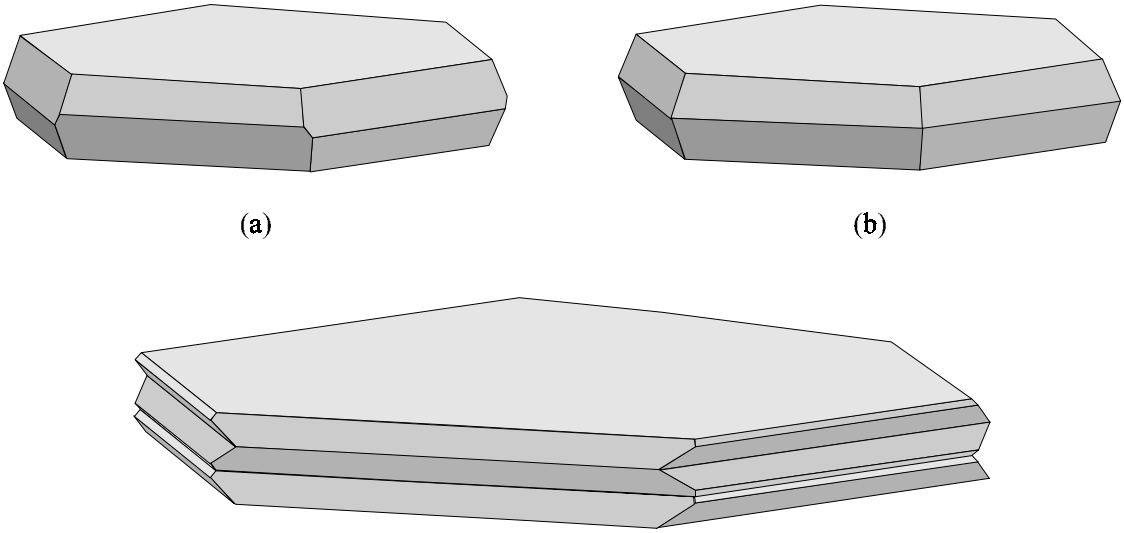

(**a**) Trigonal (point group 3m) $BaTiO_3$ crystal showing different pyramidal faces and the extremely developed {001} faces. This drawing represents a typical morphology of the observed crystals of hexagonal polymorph, grown under reducing sintering conditions.

(**b**) Hexagonal (point group 6/mmm) $BaTiO_3$ showing equally developed {101} faces with large basal {001} faces. Crystals with this morphology were never observed in the materials sintered under reducing conditions. Unit–cell parameters for both drawings were those of hexagonal $BaTiO_3$ (Akimoto et al. 1994). Crystals were reconstructed employing software for crystal drawings (SHAPE program, Dowty 1994).[43]

Hexagonal $BaTiO_3$ and parallel (111) twins of cubic phase

A comparison between the [110] projection of the hexagonal phase and the $[\bar{1}10]$ projection of the (111) twin in cubic $BaTiO_3$, shown in Figure 26, reveals a very similar crystallographic arrangement in the vicinity of the hexagonal stacking. Ti ions within face–sharing Ti_2O_9 octahedrons of such a hexagonal stacking are known to be the most favourable arrangement for the accommodation of Ti^{3+} ions. EELS results by Rečnik et al. (1994) [38] revealed the presence of Ti^{3+} along the (111) twin boundary in $BaTiO_3$.

FIGURE 26

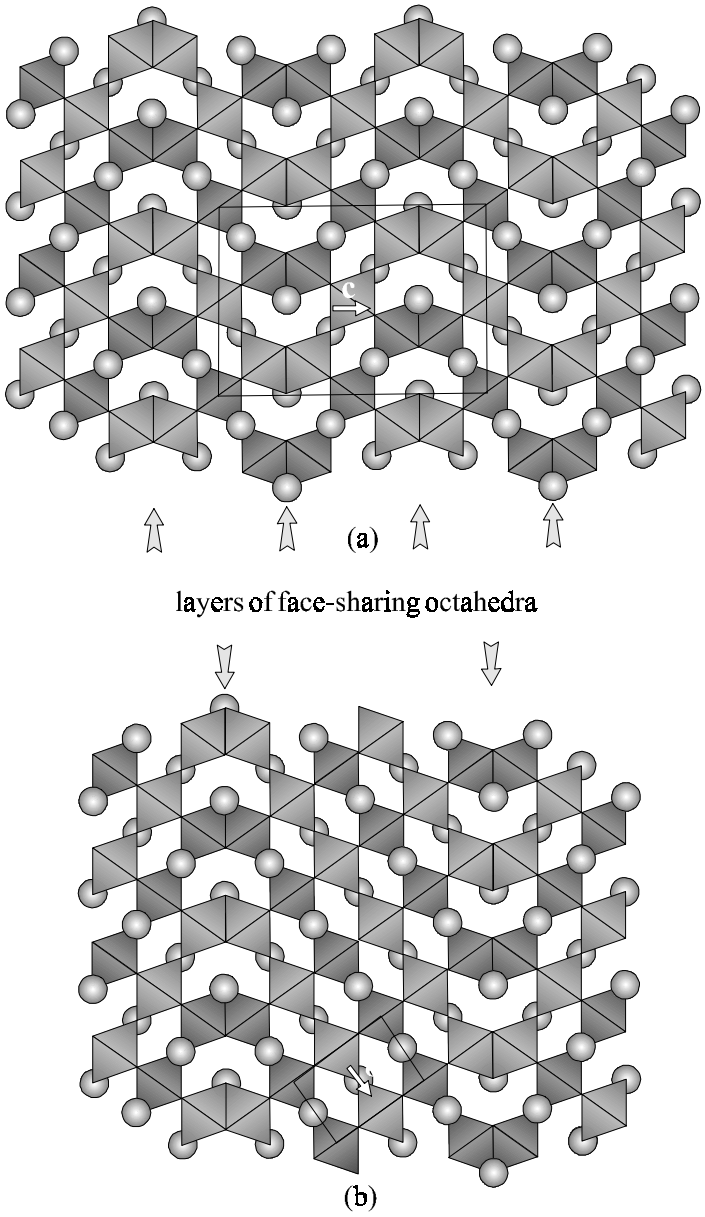

Comparison between the prism views of (**a**) hexagonal and (**b**) that of the parallel (111) twin combination in a cubic $BaTiO_3$. Note the similar crystallographic arrangement, Ti_2O_9 groups in the vicinity of the hexagonal stacking.

The presence of Ti in a lower oxidation state was considered to be the result of reducing sintering conditions. Wakamatsu et al.[27] showed that a minimum of 0.3% of Ti^{3+} is needed to stabilise hexagonal $BaTiO_3$ when prepared below the temperature of the cubic–hexagonal transition. Although there is no indication in the literature as to

where the Ti^{3+} is incorporated in the reduced modification of hexagonal $BaTiO_3$ there are no obstacles to prevent them occupying identical crystallographic sites as detected in (111) twins in the cubic phase. The exaggerated grain growth in parallel (111) twins reported by Schmelz and Thomann [3] takes place along layers of face–sharing octahedra which are the most favourable sites for the incorporation of Ti^{3+} ions.

In hexagonal $BaTiO_3$ a discontinuous growth also occurs along the layers of face–sharing octahedra at an incomparably higher growth rate since there are infinitely more *re–entrant* angles compared to the special case of double (111) twins in the cubic phase. Double (111) twins in cubic $BaTiO_3$, with the stacking sequence *ABCACB...ACBABC*, which contain only two layers of face–sharing octahedra have just a sufficient number of six nucleation sites available for crystal growth in all six <211> directions. Densification and multiplication of such layers to form polysynthetic (111) twins leads to hexagonal structure with the ...*ABCACB*... stacking, and produces a superabundance of nucleation sites for crystal growth in all six <211> directions, with respect to the cubic unit–cell.

Growth of hexagonal $BaTiO_3$ under reducing sintering conditions

The coexistence of both hexagonal and cubic $BaTiO_3$ grains is achieved in short times under reducing sintering conditions. The amount converted to the hexagonal phase increases proportionally with time. This is more clearly seen in Figure 27. Powder XRD spectra recorded for the $BaTiO_3$ ceramic show a higher yield of the hexagonal phase at longer sintering times along with a decrease in the cubic (tetragonal) fraction.

Typical microstructures developed under reducing sintering conditions above the eutectic temperature are illustrated in Figure 28. The microstructures of $BaTiO_3$ ceramic show a bimodal grain distribution. Photographs of polished cross–sections reveal the presence of elongated grains for the shortest sintering time, with their size and quantity increasing after longer firing periods. Taking into account the microstructural features and corresponding XRD data one could anticipate that the exaggeratedly grown grains are hexagonal $BaTiO_3$ (Rečnik and Kolar 1996).[41]

The exaggeratedly grown grains are also markedly anisotropic. This could be the result of a considerably higher growth rate in particular directions. The hexagonal grains

include a relatively high quantity of smaller globular grains which could be precipitates of another phase or simply grains which became trapped due to the high growth rate of the host crystal. However, this question could be resolved the TEM analysis.

FIGURE 27

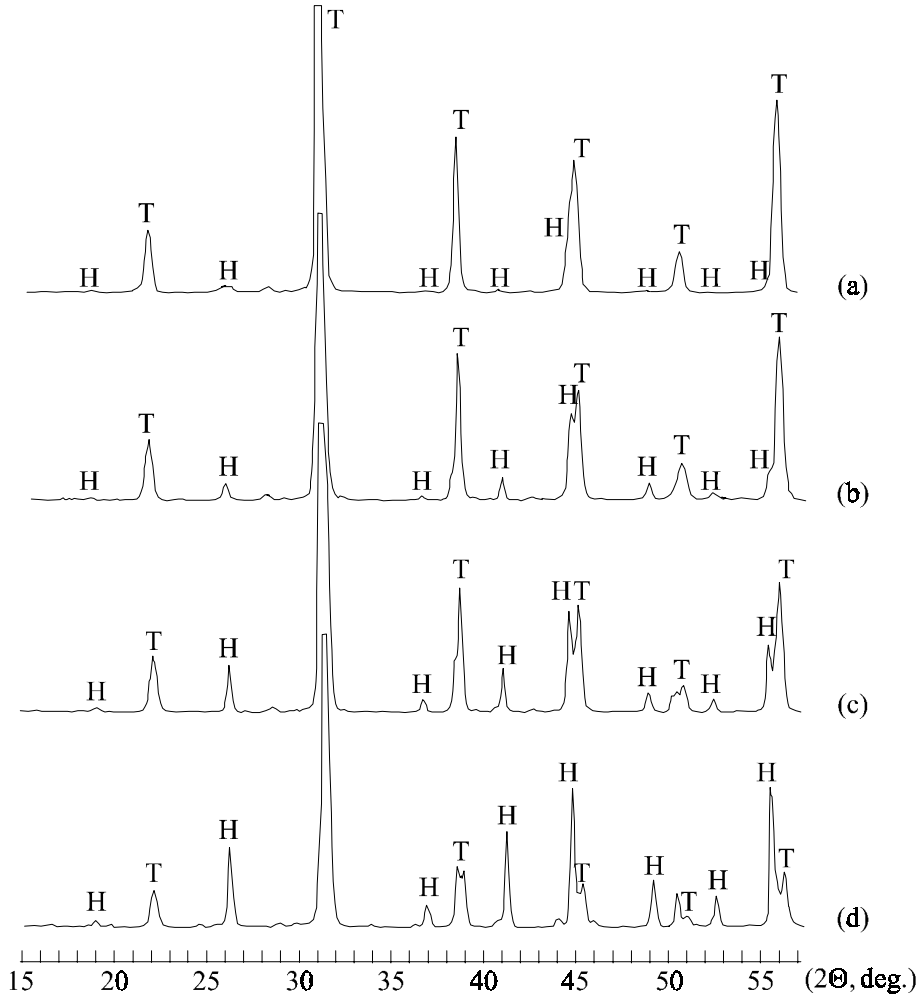

Powder XRD spectra recorded after different sintering times at 1360°C: (**a**) 5 min; (**b**) 15 min; (**c**) 30 min; and (**d**) 60 min.

In order to determine the crystallographic directions of exaggerated growth and to check for the presence of a liquid phase at the grain boundaries we used a conventional and high–resolution TEM. In the HRTEM micrographs shown in Figure 29, the sense of the c–axis of the hexagonal crystal is indicated. The c–axis orientation is perpendicular to the elongation of the grain which indicates that the exaggerated growth could occur in the direction of the {100} and $\{\bar{1}10\}$ prism planes.

FIGURE 28

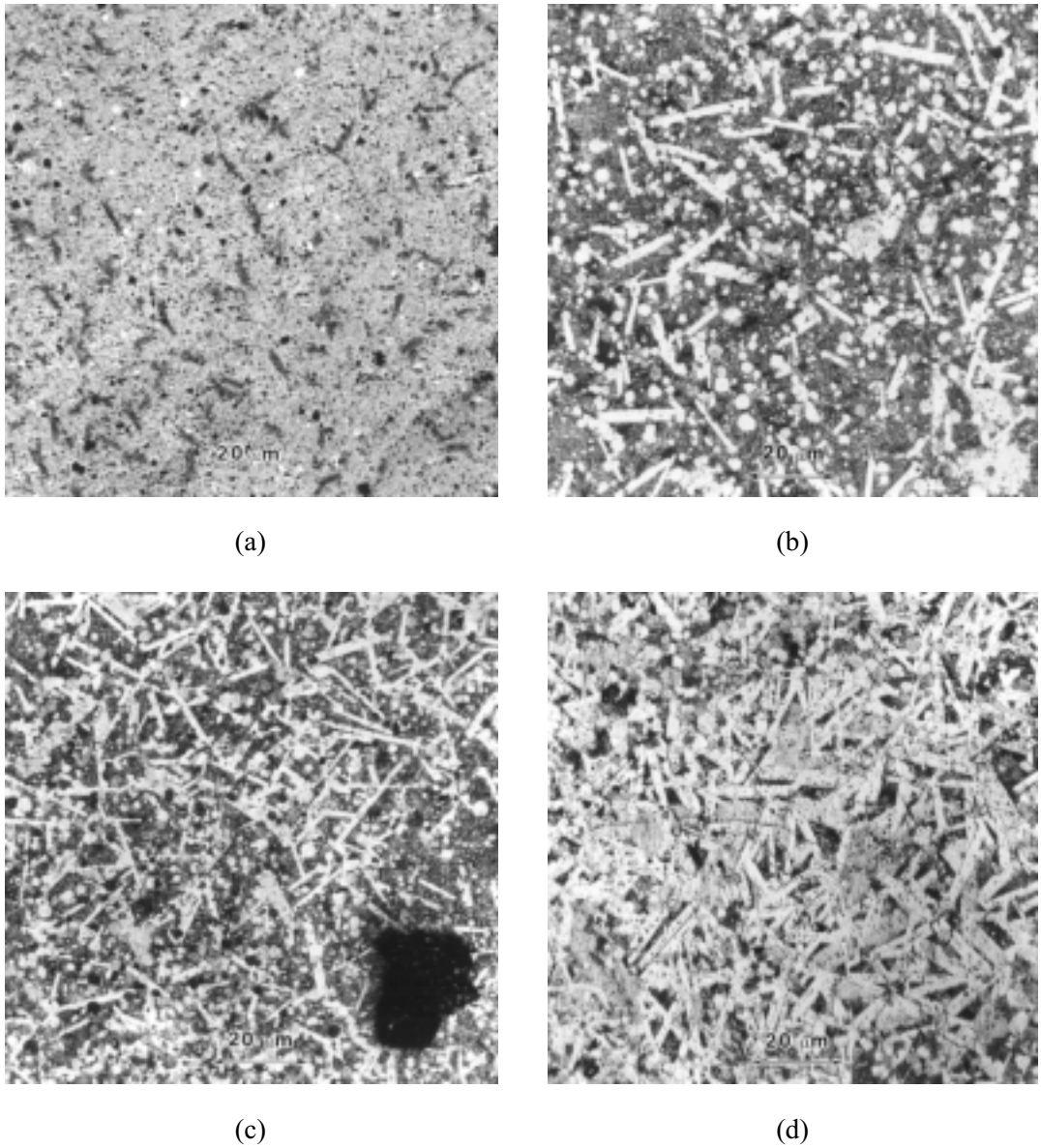

(a) (b)

(c) (d)

Optical micrographs of polished cross sections after the sintering conditions, corresponding to the XRD spectra in Figure 27, show elongated hexagonal grains within the fine grained cubic $BaTiO_3$ matrix.

At the grain boundary, running parallel to the basal planes we can observe a thin amorphous layer of Ti–rich phase which is crystallised at the triple points in the form of a $Ba_6Ti_{17}O_{40}$ –like compound. This phase could not be indexed as $Ba_6Ti_{17}O_{40}$ since the composition of this compound varies considerably under reducing sintering conditions

FIGURE 29

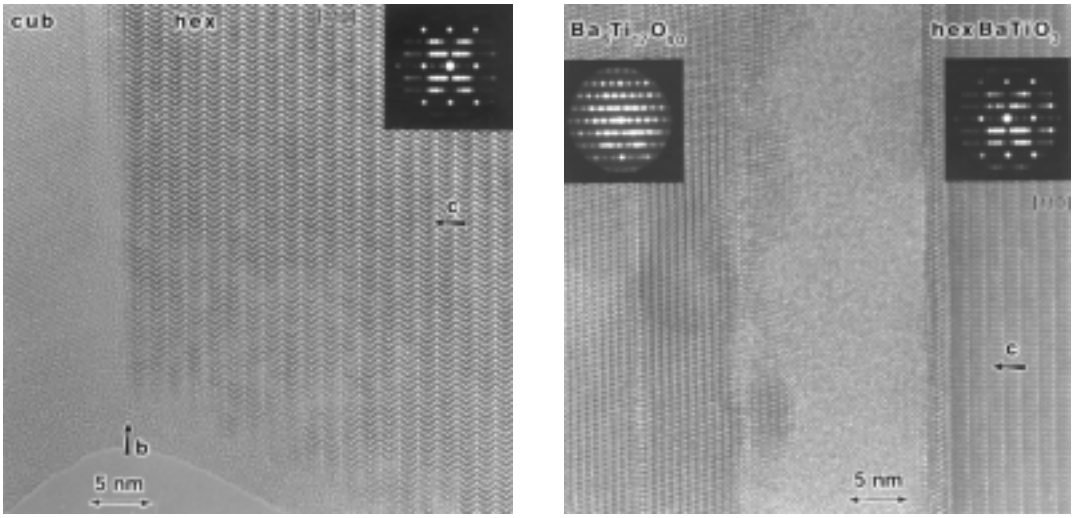

(a) (b)

(**a**) HRTEM micrograph of a cubic–hexagonal interface showing a thin amorphous layer b wetting the two crystals. This indicates a liquid–phase–assisted grain growth.

(**b**) HRTEM micrograph of a $Ba_6Ti_{17}O_{40}$ – hexagonal $BaTiO_3$ grain boundary.

(Bast et al.).[18] The coherent layers of a solidified liquid phase are also isolated from the hexagonal crystal by a thin amorphous layer. During the course of the TEM work no coherent precipitates of the cubic phase could be found in the hexagonal $BaTiO_3$ crystals and no other coherent interfaces of the cubic and hexagonal phases were observed.

A relatively high concentration of inclusions in the hexagonal grains supports the proposed mode of exaggerated growth for these grains. The majority of the inclusions are unissolved cubic grains which were overgrown by the abruptly expanding hexagonal grains. The analysis of HRTEM images at the grain boundaries confirmed the regular appearance of an at–least–6–nm–thick amorphous layer around the hexagonal grains, suggesting that the exaggerated growth of hexagonal $BaTiO_3$ is liquid–phase assisted. This enables the rapid mass transfer from cubic $BaTiO_3$ grains to the nucleation sites of hexagonal polymorph. The presence of Ti^{3+}, induced by reducing sintering conditions, is necessary for the nucleation of hexagonal stacking at lower temperatures, where cubic–hexagonal phase transition does not spontaneously occur in air. The nucleation of face–sharing octahedra and the exaggerated growth of hexagonal grains would be stopped at the moment when the firing atmosphere becomes oxidising (Rečnik and Kolar 1996).[41]

FIGURE 30

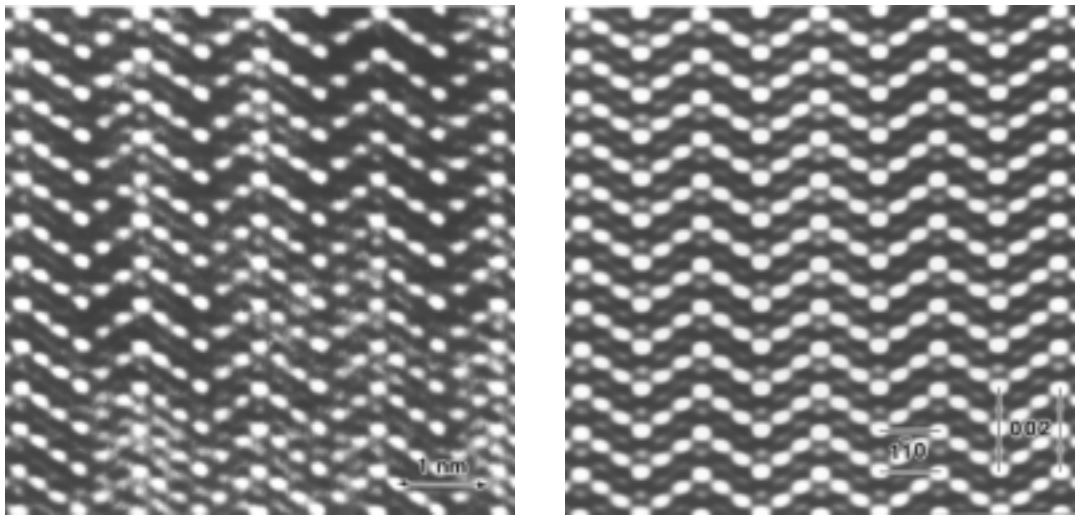

(a) (b)

(**a**) Raw and (**b**) filtered experimental lattice images of the thin crystal part from Figure 29 (a) showing a hexagonal $BaTiO_3$. Note the similarity of atomic column arrangement with that in lattice images 10 and 11 showing a (111) twin in cubic $BaTiO_3$.

A symmetry reduction

The observed lower symmetry of the exaggeratedly grown $BaTiO_3$ crystals may be a consequence of the Ti^{3+} incorporated in the hexagonal crystal lattice accompanied by the loss of an equilibrium quantity of oxygen. Large Ti^{3+} ions and corresponding oxygen vacancies affect the internal crystal symmetry in such a manner that a six–fold axis along the [001] direction is replaced by a three–fold screw axis. The most favourable environment for the Ti^{3+} incorporation are the Ti sites in the Ti_2O_9 coordination groups (similar to those along the cubic twin boundary). The loss of hexagonal symmetry can be assigned to minute atomic displacements caused by the larger Ti^{3+} ions in these sites, with the coordination preserved throughout the crystal (Rečnik and Kolar).[44-45]

In order to replace all the Ti^{4+} ions in the face–sharing octahedrons with Ti^{3+} the composition of the hexagonal $BaTiO_3$, having 2/3 of Ti atoms located in these groups, would be $BaTi^{4+}_{1/3}Ti^{3+}_{2/3}O_{3-1/3}O^{\cdot\cdot}_{1/3}$. This might cause severe changes to the hexagonal perovskite unit cell. Such an oxygen–deficient barium titanate has never been observed, which agrees with the findings of Wakamatsu et al.[27] that there is a small quantity of Ti^{3+} needed to stabilise the hexagonal phase at low temperatuers. Rečnik et al.[38] reported

that for (111) twin boundaries only a partial substitution of Ti^{4+} ions by Ti^{3+} in Ti_2O_9 groups takes place.

A partial reduction of Ti^{4+} ions in face–sharing coordination groups would result in $BaTi^{4+}_{1-2x}Ti^{3+}_{2x}O_{3-x}O^{\cdot\cdot}_x$ for the composition of hexagonal $BaTiO_3$. There is a slight possibility, however, for a gradual increase in atomic displacements, resulting in smooth transition from the stiochiometric $BaTiO_3$ to $BaTi^{4+}_{1/3}Ti^{3+}_{2/3}O_{3-1/3}O^{\cdot\cdot}_{1/3}$, depending on a degree of reduction of individual grains.

Summary and Conclusions

Several problems related to the exaggerated grain growth in $BaTiO_3$ have been addressed in this study. It has been shown, that the local structure of (111) twins in cubic $BaTiO_3$ is strongly influenced by the reducing sintering conditions. On the basis of these observations a nucleation mechanism for these defects has been proposed. In conclusion, it has been shown that the formation of the hexagonal polymorph is closely related to that of the (111) twins in the cubic polymorph of $BaTiO_3$. In past few years, many studies related to the structure of (111) twins in $BaTiO_3$,[46-53] nucleation and their role in exaggerated grain growth [54-60] can be found in the literature.

The local structure of the (111) twin boundary in cubic $BaTiO_3$

A new structural model for the coherent (111) twin boundary in cubic $BaTiO_3$ is proposed on the basis of quantitative HRTEM and spatially resolved EELS analysis:

- The (111) twin in $BaTiO_3$ is a coherent twin with a $Ba–O_3$ close–packed plane at the interface. Ti atoms adjacent to the twin boundary plane are octahedrally coordinated with the octahedra sharing faces. The Ti–Ti bond length in the face–sharing octahedrons is 0.234 nm ±0.02 nm. This is lower than the Ti–Ti bond length in the face–sharing octahedra reported for hexagonal polymorph of $BaTiO_3$. The contraction of the bond length is likely to be due to the presence of Ti ions having a lower oxidation state than 4+ at these sites.
- The interface plane should be oxygen deficient to balance the charge of the Ti ions adjacent to the boundary plane. A chemical composition of the boundary

plane is therefore $Ba–O_{3–x}[O¨]_x$ instead of $Ba–O_3$ and hence the composition of the face–sharing octahedra becomes $[(Ti^{4–x})_2O_{9–x}(O¨)_x]^{10–}$ instead of $[Ti_2O_9]^{10–}$.

- The change in the interface chemistry can be understood as a consequence of the reducing sintering conditions. This is a strong indication that (111) twins in $BaTiO_3$ are formed as growth defects. No other structural types of (111) twins have been observed.

Nucleation mechanism of (111) twins under reducing conditions

With the determination of the (111) twin local structure it has been shown that the reducing conditions play an important role in the formation of the twin. Furthermore, it has been found that they form at a very early stage of sintering. Using this information a probable nucleation mechanism for the (111) twins is proposed:

- The exposed octahedral faces of original $BaTiO_3$ crystals undergo a reduction process. Consequently, an equilibrium quantity of O from the $Ba–O_3$ close–packed surface layers is removed. The charge is compensated by a reduction of the neighbouring Ti layers. An O–deficient $Ba–O_2O¨$ layer is an obstruction to the normal growth of $BaTiO_3$. The next layer of Ti atoms deposited on such a surface accommodates in a position for the face–sharing octahedrons.
- At higher temperatures, when diffusion in the solid state occurs, the material deposited on such surfaces grows, because of the faulted surface structure and to retain the local charge balance, in the only possible – twinning orientation with respect to the original $BaTiO_3$ crystal.
- In this way, regarding the morphology of the original crystallite, either single twins, or *parallel*, *obtuse* and *acute* twin combinations may form. However, more complex twin combinations are for the case when the original crystallite is already twinned.

Formation of the hexagonal $BaTiO_3$ under reducing conditions

Barium titanate processed under reducing sintering conditions above the eutectic temperature exhibits characteristic anomalously grown grains of hexagonal $BaTiO_3$. The following observations have been made:

- The abnormal growth of hexagonal crystallites above the eutectic temperature is similar to the exaggerated growth of *parallel* (111) twins of the cubic phase below the eutectic temperature. Grain growth is liquid–phase assisted.
- Considering the crystallographic directions of discontinuous growth along the face–sharing octahedrons the phenomenon of the parallel (111) twins can be explained as a preparatory stage for the hexagonal phase.
- Ti^{3+} ions are understood to initiate the formation face–sharing octahedra in the form of Ti_2O_9 groups which are nucleation sites for the hexagonal stacking. As long as the firing atmosphere allows the formation of the oxygen vacancies, and hence the Ti^{3+} ions are established for the charge balance, the nucleation of a hexagonal stacking would be preferred.
- Hexagonal crystallites have a distorted hexagonal perovskite–related structure due to the incorporation of Ti^{3+} ions in the Ti_2O_9 groups. Slight atomic shifts caused by a different chemical environment destroy six–fold symmetry along the [001] direction which is replaced by a three–fold screw axis. The symmetry of a reduced hexagonal $BaTiO_3$ is trigonal 3m rather than hexagonal 6/mmm. Regardless the symmetry change coordination of the atoms remains preserved.

Acknowledgement

This research was carried out during the period 1991–2000 in collaboration with prof. dr. Drago Kolar, with whom I shared a common interest in studying the influence of (111) twins on the exaggerated grain growth in $BaTiO_3$ ceramics. Over the last few years we further developed the general concept of the formation of the planar faults as a preparatory stage of reconstructive phase transformations. Furthermore, we found that this type of the planar fault triggers abnormal grain growth in ceramics, and while it is often advantageous to avoid exaggerated grain growth, many situations exist where it is possible to exploit this effect to design textures with specific crystal morphologies.

This concept may represent only a small part of the scientific work in which prof. Kolar was engaged, and yet it is of fundamental importance for the scientific community dealing with the phenomenon of crystal growth. I wish to express my joy and gratitude at having had the chance to work with him.

References

1. O. Eibl, P. Pongratz, P. Skalicky and H. Schmelz, *J. Am. Ceram. Soc.* **1987**, 70, 195.
2. H. Oppolzer and H. Schmelz, *J. Am. Ceram. Soc.* **1983**, 66, 44.
3. H. Schmelz and H. Thomann, *Ceram. Forum Int.* **1984**, 61, 199.
4. G. Kästner, R. Wagner, G. Lacayo and V. Hilarius, *J. Mat. Sci. Letters* **1989**, 8, 802.
5. H. D. Megaw, *Proc. Roy. Soc. (London)* **1947**, 189, 261.
6. J.W. Edwards, R. Speiser and H. L. Johnston, *J. Am. Chem. Soc.* **1951**, 73, 2934.
7. J. Harada, T. Pedersen and Z. Barnea, *Acta Cryst. A* **1970**, 26, 336.
8. E. A. D. White, *Acta Cryst.* **1955**, 8, 845.
9. J. P. Remika, *J. Am. Chem. Soc.* **1954**, 76, 940.
10. R.C. DeVries and J. E. Burke, *J. Am. Ceram. Soc.* **1957**, 40, 200
11. H. Blank and S. Amelinckx, *Appl.Phys.* **1963**, 2, 140.
12. D. Hennings, *Int. J. High Techn. Ceram.* **1987**, 3, 91.
13. J. Akimoto, Y. Gotoh and Y. Oosawa, Acta Cryst. C **1994**, 50, 160.
14. R. D. Burbank and H. T. Evans, *Acta Cryst.* **1948**, 1, 330.
15. K. W. Kirby and B. A. Wechsler, *J. Am. Ceram. Soc.* **1991**, 74, 1841.
16. R. M. Glaister and H. F. Kay, *Proc. Phys. Soc.* **1960**, 76, 763.
17. E. Tillmanns and W. H. Baur, *Acta Cryst. B* **1970**, 26, 1645.
18. U. Bast, G. Tomandl and L. Hanke, *Silicates Industriels* **1984**, 9, 191.
19. D. B. Jugle, *Ph.D. Thesis (Ransselear Polytec. Inst., Troy, NY)*, **1966**.
20. O. Eibl, P. Pongratz and P. Skalicky, *Phil. Mag. B* **1988**, 57, 521.
21. L. A. Bursill, M. G. Blanchin, A. Mebarek and D. J. Smith, *Rad. Effects* **1983**, 74, 253.
22. R. W. Cahn, *Advances in Physics. Supplement of the Philos. Magazine* **1954**, 3, 363.
23. V. Kraševec, M. Drofenik and D. Kolar, *J. Am. Ceram. Soc.* **1990**, 73, 859.
24. V. Kraševec and A. Prodan, *Beitr. Elektronenmikr. Direktabb. Oberfl.* **1983**, 16, 263.
25. H. Schmelz and A. Meyer, *Ceram. Forum Int.* **1982**, 59, 436.
26. H. Schmelz and H. Thomann, *Ceram. Forum Int.* **1984**, 61, 199.
27. M. Wakamatsu, N. Takeuchi, G. C. Lai and S. Ishida, *Yogyo–Kyokai–Shi* **1987**, 95, 1181.
28. F. Zemlin, *Ultramicroscopy* **1979**, 4, 241.
29. P. A. Stadelmann, *Ultramicroscopy* **1987**, 21, 131.
30. G. Möbus, G. Necker and M. Rühle, *Ultramicroscopy* **1993**, 49, 46.
31. J. Bruley, *Microsc. Microstr. & Microanalysis* **1993**, 4, 23.
32. R. D. Leapman, L. A. Grunes and F. J. Fejes, *Phys. Rev. B* **1982**, 26, 614.
33. M. T. Otten, B. Miner, J. H. Rask and P. Buseck, *Ultramicroscopy* **1985**, 18, 285.
34. M. Sankararaman and D. Perry, *J. Mat. Sci.* **1992**, 27, 2731.
35. R. Brydson, *EMSA Bulletin* **1991**, 21, 57.
36. F. DeGroot, J. C. Fuggel, B. T. Thole and G. A. Sawatzky, *Phys. Rev. B* **1990**, 41, 928.
37. J. Bruley, A. Rečnik and W. Mader, *MRS Meeting (Boston)*, **1993**.
38. A. Rečnik, J. Bruley, W. Mader, D. Kolar and M. Rühle, *Philos. Magazine B* **1994**, 70, 1021.
39. A. Rečnik and D. Kolar, *Micr. Electronica (Parma)* **1993**, 14, Suppl.2, 283.

40. L. Ramqvist, K. Hamrin, G. Johansson, A. Fahlman and C. Nording, *J. Phys. & Chem. of Solids* **1969**, 30, 1835.
41. A. Rečnik and D. Kolar, *J. Am. Ceram. Soc.* **1996**, 79, 1015.
42. D. Kolar, U. Kunaver, A. Rečnik, *Physica Status Solidi (a)* **1998**, 166, 219.
43. E. Dowty, *SHAPE (crystal drawing program)*, **1994**.
44. A. Rečnik and D. Kolar, *J. Computer Assisted Microscopy* **1997**, 9, 51.
45. A. Rečnik and D. Kolar, *Acta Chim. Slov.* **1995**, 42, 219.
46. E. Hamada, W. S. Cho and K. Takayanagi, *Philos. Magazine A* **1998**, 77, 1301.
47. C. L. Jia, R. Rosenfeld, A. Thust and K. Urban, *Philos. Magazine Lett.* **1999**, 79, 99.
48. M. A. McCoy, W. E. Lee, R. W. Grimes and R. Keyse, *J. Mater. Sci.* **1998**, 33, 5759.
49. S. Stemmer, S. K. Streiffer, N. D. Browning and A. I. Kingon, *Appl. Phys. Lett.* **1999**, 74, 2432.
50. C. L. Jia and A. Thust, *Phys. Rev. Lett.* **1999**, 82, 5052.
51. C. H. Lei, C. L. Jia, M. Seigert and K. Urban, *Philos. Magazine Lett.* **2000**, 80, 371.
52. B. Jiang, J. L. Peng, L. A. Bursill, T. L. Ren, P. L. Zhang and W. L. Zhong, *Physica B* **2000**, 291, 203.
53. T. Suzuki, Y. Nishi and M. Fujimoto, *J. Am. Ceram. Soc.* **2000**, 83, 3185.
54. C. L. Jia, K. Urban, M. Mertin, S. Hoffmann and R. Waser, *Philos. Magazine A* **1998**, 77, 923.
55. W. S. Cho, *J. Phys. Chem. Solids* **1998**, 59, 659.
56. C. L. Jia, K. Urban, S. Hoffmann and R. Waser, *J. Mater. Res.* **1998**, 13, 2206.
57. M. H. Lin, J. F. Chou and H. Y. Lu, *J. European Ceram. Soc.* **2000**, 20, 517.
58. H. Y. Lee, J. S. Kim, N. M. Hwang and D. Y. Kim, *J. European Ceram. Soc.* **2000**, 20, 731.
59. B. K. Lee, S. Y. Chung and S. J. L. Kang, *Metals and Materials (Korea)* **2000**, 6, 301.
60. A. Rečnik, M. Čeh and D. Kolar, *J. European Ceram. Soc.* **2001**, 21, in press.

Povzetek

Na primeru (111) dvojčkov v kubični modifikaciji barijevega titanata ($BaTiO_3$) je prikazano, da lahko redukcijsko okolje sintranja izredno poveča težnjo kristalov k tvorbi dvojčkov, i.e. k tvorbi heksagonalnega zloga v obliki Ti_2O_9 koordinacijskih skupin. Te skupine so namreč lastne tako (111) dvojčkom v kubični, kakor tudi sami heksagonalni modifikaciji $BaTiO_3$. V znanstveni literaturi ni bilo znanih eksperimentalnih dokazov, ki bi osvetlili dejansko naravo ali mehanizem kubično–heksagonalne fazne transformacije v $BaTiO_3$. Fazno transformacijo lahko s procesiranjem v redukcijskih pogojih premaknemo daleč pod normalno temperaturo faznega prehoda, kar kaže na to, da lahko z ustreznim kemijskim okoljem kontroliramo prehod iz ene v drugo modifikacijo ter da so dvojčki v kubičnem $BaTiO_3$ le pripravljalna stopnja kubično–heksagonalne fazne transformacije.